Electronic structure of the ordered phases of Pt-Fe alloys

Marek Podgórny
Instytut Fizyki, Uniwersytet Jagiellonski, PL-30-059 Kraków, Reymonta 4, Poland
and Institut fur Theoretische Physik III, Ruhr Universität, Bochum, Universitätstrasse 150, Germany
(Received 20 July 1990)

The electronic structure of several ordered phases of the Pt-Fe system is studied using the self-consistent linear muffin-tin-orbital method. The phases studied include nonmagnetic and ferromagnetic $PtFe_3$, ferromagnetic Pt_2Fe_2, antiferromagnetic and ferromagnetic Pt_3Fe, and ferromagnetic Pt_5Fe_3. The electronic structure, the densities of states, and the ground-state properties, such as equilibrium lattice constants, bulk moduli, local and average magnetic moments, and the state equations are calculated. The calculated parameters compare favorably with existing experimental data. The cohesive properties, chemical bonding, and the moment-stabilizing mechanism are discussed. A variation of all these aspects with alloy composition illustrates a continuous transition from itinerant to local-moment magnetism. An interplay of the covalent bonding, scalar relativistic effects, electronegativity, and the charge transfer is shown to be responsible for this transition. Homogeneity of the magnetic state of $PtFe_3$ Invar is explained. On the basis of the calculated elastic properties and recently reported critical pressures at which the magnetic moment of $PtFe_3$ collapses, the total energy difference between the ferromagnetic and nonmagnetic phase is estimated.

I. INTRODUCTION

The Pt-Fe system possesses many interesting physical properties. It has a continuous range of solid solutions, and both stoichiometric and nonstoichiometric alloys with various degrees of order can be prepared. At Fe concentrations larger than approximately 25 at. %, the ordered and disordered samples have a fcc lattice and, for lower Fe concentrations, a martensitic transformation to the bcc phase occurs. The ordered phases of $PtFe_3$ and Pt_3Fe of $AuCu_3$ type and of Pt_2Fe_2 of AuCu I type can be grown, although because of the martensitic transformation, the material customarily referrred to as ordered $PtFe_3$ usually has one slightly different composition of $Pt_{28}Fe_{72}$. Of these phases, the most celebrated is $PtFe_3$ (Refs. 1–6): it is an Invar material showing very strong anomalies in the thermal-expansion coefficient and spontaneous volume magnetostriction, yet no deviation from the Slater-Pauling curve, no anomalies of lattice constant, and no mixed magnetic or reentrant spin-glass behavior at low temperatures.[6–9] $PtFe_3$ is considered to be a hard homogeneous ferromagnetic material.[6] A discovery of its Invar anomalies[1] played an important role for the present understanding of Invar problems. Many of the Invar theories put forward in the past proposed mechanisms such as chemical disorder,[10] latent antiferromagnetism,[11] weak ferromagnetism,[12] magnetic inhomogeneity,[13] or short-range-order influence.[14] All of these theories can now be discarded. It seems that, recently, some consensus has been reached as to the basic physics of Invar materials:[15,7–9] it is believed that, at $T=0$, there are two energetically nearly degenerate states of such a system, a high-spin (HS) state, with a large magnetic volume, and a low-spin (LS) state (which may, but need not, be nonmagnetic) with a smaller volume. A small total-energy difference is essential,[15] but no direct calculation of its value seems to have been published up to now for any existing Invar material. In any case, it seems that this energy must be in the thermal range to allow for appreciable longitudinal spin fluctuations.

Although $PtFe_3$ is considered a hard ferromagnet, the itinerant character of the magnetism in this material is self-evident. The Pt_3Fe phase is a substance close to the local-moment limit.[16] It seems to us that a study of the electronic structure of the Pt-Fe system as a function of composition is an exciting venture. A possible microscopic origin of such a transformation upon composition change will be investigated in this paper. In spite of the very interesting properties of the Pt-Fe alloys briefly outlined above, there are only very few theoretical calculations of their electronic structure. Pettifor and Roy[17] considered the magnetovolume instability in $PtFe_3$ using the canonical band theory, and Inoue and Shimizu[18] calculated the electronic structure of $Pt_{1-x}Fe_x$ for $0.25<x<0.32$ using an empirical tight-binding approach and coherent-potential approximation. The self-consistent studies known to us include the spin-polarized calculations of $PtFe_3$ electronic structure carried out by Hasegawa[19(a)] and the paramagnetic band-structure calculations of Pt_3Fe reported by Kulikov *et al.*[19(b)] Both studies were limited to the experimental lattice constants. The total energy of $PtFe_3$ as a function of both atomic volume and magnetic moment was calculated by Moruzzi *et al.*[20] in an unpublished work. The very recent calculation of Entel and Schröter[21] used the binding surface calculated by Moruzzi *et al.*,[20] modified in an arbitrary way in order to shift the nonmagnetic saddle point above the ferromagnetic minimum, to describe the spin fluctuations in $PtFe_3$. Other compositions were not considered, and such problems as chemical bonding, cohesive properties,

state equations, and magnetic-moment stabilization and enhancement mechanisms were never addressed.

In this paper, we report on an extensive study of the electronic structure and related properties of the Pt-Fe system in the fcc phase. The paper is organized as follows: in Sec. II, we briefly summarize the computational details; in Sec. III, we present the equilibrium band structures and densities of states (DOS's) for $PtFe_3$, Pt_2Fe_2, and Pt_3Fe. Further, local and average magnetic moments and their volume dependencies are discussed there. Cohesive properties and chemical bonding are discussed in Sec. IV. Section V discusses hyperfine-field compositions dependence, magnetic homogeneity of $PtFe_3$, and the total-energy difference between the ferromagnetic and nonmagnetic phases of this material. Section VI contains a summary.

II. METHOD OF CALCULATION

We have used the well-known linear muffin-tin-orbital (LMTO) method of band-structure calculation.[22] The method is described in detail elsewhere,[23] so we will limit ourselves here to a description of specific details of the present calculations. We have used the Vosko-Wilk-Nusair[24] exchange-correlation potential and the frozen-core approximation. The combined correction terms[22] have been used in all calculations, whereas the f orbitals have not. The scalar relativistic terms have been included in the radial Schrödinger equation solved within atomic spheres. The ratio of the atomic-spheres radii S_{Pt}/S_{Fe} has been set to 1.084 079 and kept constant throughout the series of calculations. The value follows from the ratio of atomic volumes of elemental Pt and Fe in their ground states. At this ratio, there is always a small charge transfer between the spheres (properly taken into account via the Madelung matrix). The charge transfer is composition and volume dependent, and there is no way to find a universal S_{Pt}/S_{Fe} ratio at which the charge transfer vanishes for all alloy compositions. It will be shown that composition dependence of the charge transfer is an important physical factor.

For nonmagnetic (NM) and ferromagnetic (FM) phases of $PtFe_3$ and Pt_3Fe, the calculations have been carried out for the $AuCu_3$ symmetry (simple cubic lattice, space group O_h^1); for Pt_2Fe_2, the symmetry taken was AuCu I (primitive tetragonal, $c/a=1$, space group D_{4h}^1). The calculations for the antiferromagnetic (AF) Pt_3Fe have been carried out for AFIII ordering, and the symmetry was primitive tetragonal, $c/a=2$, space group D_{4h}^1, the same as for the hypothetical ordered Pt_5Fe_3. This last supercell will be discussed further in Sec. III C. For all of the FM phases, the calculations have been carried out for atomic volumes of $(0.7-1.1)V_{eq}$. The number of **k** points used for Brillouin-zone integration varied from one structure to another, but it was never smaller than 286 points per irreducible wedge.

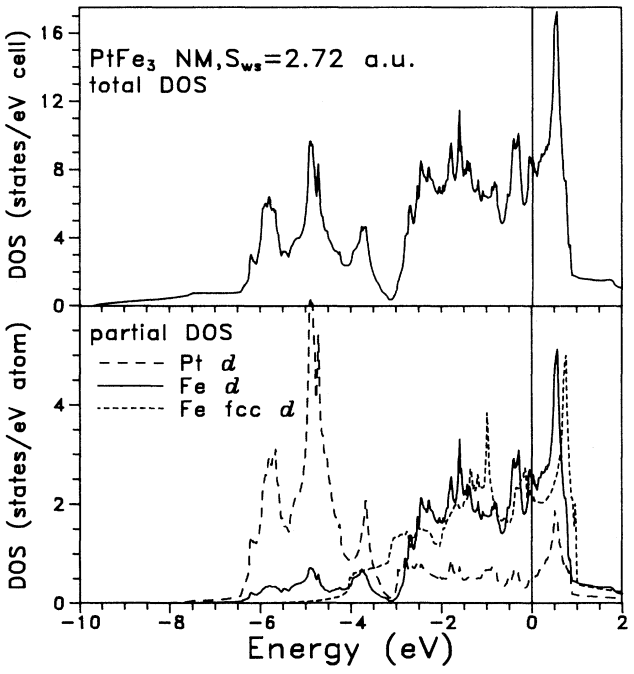

FIG. 1. Density of states for nonmagnetic $PtFe_3$ at $S_{WS}=2.72$ a.u. The upper panel is the total DOS, and the lower panel is the partial d DOS for Pt and Fe. Additionally, d DOS for fcc Fe at the same lattice constant is plotted. Note the different DOS units in upper and lower panel.

III. ELECTRONIC STRUCTURES AT EQUILIBRIUM

A. Nonmagnetic $PtFe_3$

For $PtFe_3$, the calculations have been carried out for both NM and FM phases as a function of atomic volume. The calculated equilibrium Wigner-Seitz radii (see Sec. IV) S_{WS} for these phases are 2.67 and 2.726 a.u., respectively [the lattice constant a (Å)$=0.529(16\pi/3)^{1/3}S_{WS}$ (a.u.)$=1.3536S_{WS}$ (a.u.)]. In Fig. 1, the most important DOS features for NM $PtFe_3$ at $S_{WS}=2.72$ a.u are shown. In this, and in all subsequent figures displaying DOS's, the energy scale has been shifted so that the Fermi energy falls at 0. The upper panel shows the total DOS, and the lower panel shows the Pt d and Fe d components. They are normalized to the (states per eV and atom) units. We will discuss this picture in more detail, for it is essential for understanding the main features of the electronic structure of the Pt-Fe system. An important problem in this context is why the $PtFe_3$ is ferromagnetic, i.e., what is the moment-stabilizing mechanism for this alloy composition and how does it change with a growing Pt content. An often expressed view (see, for instance, Ref. 9) is that the Fe magnetic moment in $PtFe_3$ is stabilized simply by a larger lattice spacing of the compound as compared with elemental Fe. On the other hand, it was tacitly assumed in a few recent discussions[9,25] that a moment-instability pattern for $PtFe_3$ should be similar to that of fcc Fe.[26–28] This, however, implies thinking in terms of the rigid-band model. If the magnetic moment in $PtFe_3$ is stabilized by a large lattice constant of this compound, what, then, is a moment-stabilizing mechanism in the isoelectronic Ni-Fe system, for which the lattice constant

is always smaller than that corresponding to $S_{WS}=2.68$ a.u., at which the magnetic moment of fcc Fe becomes unstable?[26] Are these mechanisms similar, and are they relevant to the Invar anomalies? We will try to clarify these problems here for the Pt-Fe system and, in another paper, for Ni-Fe.[29] A preliminary discussion of the subject has been given in Ref. 30.

As clearly seen in the lower panel of Fig. 1, the upper part of the valence band is dominated by Fe-derived states, whereas Pt states build up the lower part. This reflects a higher binding energy of the atomic Pt 5*d* shell as compared with the Fe 3*d* shell. Although there is a significant hybridization, one is still able to recognize two subbands of mainly Pt (-8–-3 eV) and Fe (-3–$+1$ eV) character. The third curve plotted in Fig. 1 is the fcc Fe DOS calculated at the same lattice constant. One notes the following.

(a) The overall shape of the Fe DOS in the elemental fcc phase and in $PtFe_3$ is quite different due to Pt-Fe hybridization. A most significant difference is a sharp maximum in the compound DOS just at the Fermi energy. This maximum is absent in the fcc Fe DOs. Its presence in the compound DOS enhances the density of states at the Fermi level by $\sim 20\%$ for $PtFe_3$ in comparison with fcc Fe. For a substance on the verge of the magnetic instability, it is a significant change.

(b) The covalency effect plays no significant role for $PtFe_3$. This effect has been shown to be responsible for enhancement of magnetism in bcc Fe-Co alloys.[31] It has also been suggested that it is important for moment enhancement in the fcc Fe-Ni system.[15] By the "covalency effect," in the context of intermetallic alloys, one understands a redistribution of weights of partial state densities in a common band formed in an alloy by atomic states having different binding energies. Arguing in the language of bonding and antibonding molecular orbitals, or using charge neutrality arguments, Schwarz *et al.*[31] demonstrated that the weight of the lower- (higher-) lying atomic states will be enhanced in the lower (upper) part of the alloy band. An enhancement of the DOS amplitude in the upper part of the band, close to the Fermi level may trigger a magnetic instability or simply enhance the magnetic moment. However, this mechanism is only effective if the distance between the parental atomic levels is small as compared with the bandwidth. This can be seen if one considers the opposite limit, namely, well-separated bands: in such a case, the weak hybridization reduces the weight of the parental atomic state in its band. The case of $PtFe_3$ is just in the intermediate regime, and the covalency and hybridization effects largely cancel. As demonstrated by a direct comparison with the fcc Fe DOS, the amplitude of the Fe states in the compound is not enhanced as compared with the elemental metal. An eventual covalency effect is canceled by a transfer of electronic states from the upper part of the band to the low-energy region dominated by Pt *d* states, i.e, to the region that would remain inaccessible to Fe *d* states in absence of Pt atoms.

A simple analysis of bandwidths (Table I) shows that an increase of the lattice constant *per se* is not necessarily responsible for magnetic instability in $PtFe_3$.

TABLE I. The bandwidths (in mRy) of Pt and Fe *d* bands for the ordered nonmagnetic $PtFe_3$ and fcc Fe at $S_{WS}=2.68$ a.u. and for fcc Fe and Pt at calculated equilibrium lattice constants. μ is the effective mass in units of m_0, W is the estimate based on the canonical band theory [Eqs. (7)–(9)], A-B is the self-consistently calculated bandwidth, η is the $(A\text{-}B)/W$, and $\bar{\eta}$ is the "ideal ratio" (see text).

Atom	μ	W	A-B	η	$\bar{\eta}$
		$PtFe_3$, NM, $S_{WS}=2.68$ a.u.			
Pt	5.02	96	563	5.86	23/2.9=7.93
Fe	9.27	267	377	1.41	23/19=1.21
		fcc Fe, NM, $S_{WS}=2.68$ a.u			
Fe	10.10	318	332	1.04	
		fcc Fe, NM, $S_{WS}=2.55$ a.u.			
Fe	8.86	399	416	1.04	
		fcc Pt, $S_{WS}=2.975$ a.u.			
Pt	5.77	450	462	1.03	

(Throughout the paper we use, unless otherwise indicated, the difference $A-B$ as a measure of a self-consistently calculated bandwidth, where A and B are band top and band bottom and may be readily calculated from other potential parameters.[23] Physically, the A and B energies correspond to the points where the logarithmic derivative of the radial wave function equals $-\infty$ and 0, respectively.) The bandwidth of the Fe *d* states in $PtFe_3$ at $S_{WS}=2.68$ a.u. equals 377 mRy, as compared with 332 mRy for fcc Fe at the same lattice constant. Also, as discussed in Ref. 30, the bandwidths of spin-polarized bands of $PtFe_3$ at equilibrium ($S_{WS}=2.726$ a.u.) correspond almost exactly to the bandwidths of the HS phase of fcc Fe at $S_{WS}=2.68$ a.u. A large atomic radius of Pt 5*d* shell increases both the lattice constant and the Pt 5*d*–Fe 3*d* wave-function overlap and, hence, the Fe *d* bandwidth. Since these effects compensate each other to a certain extent (not *a priori* known), it is not possible to establish a clear picture of the subtle balance among the lattice constant, *d* bandwidth, and magnetic moment without explicit self-consistent calculations. We realize from Table I that the Fe *d* bandwidth in $PtFe_3$ at equilibrium is larger in fcc Fe at the same lattice constant but smaller than in fcc Fe at equilibrium, and that the opposite is true for the Pt *d* bandwidth.

There is a simple method based on the canonical band theory[32] that enables one to analyze the influence of hybridization on the bandwidth. The bandwidth W_{tl} of the unhybridized band of atom t and orbital moment l is given by[32]

$$W_{tl}=\left[\frac{12}{n_{tl}}|S_{tl}^{tl}|^2\right]^{1/2}\Delta_{tl} \tag{1}$$

and

$$\Delta_{tl}=1/[\mu_{tl}S_t^2(S/S_t)^{2l+1}]\ , \tag{2}$$

where $n_{tl}=(2l+1)n_t$; n_t is the number of t-type atoms in the unit cell; S_t is the radius of the t-type atomic sphere,

μ_{tl} is the effective-mass parameter, and $|S_{tl}^{tl}|^2$ is the second moment of the canonical tl band, an expression for which can be found in Ref. 33, Eq. (22). S is a certain length, characteristic for the lattice and proportional to the lattice constant. In the present case the lattice underlying all of the considered structures is the fcc lattice, and S is set equal to the average Wigner-Seitz radius:

$$S=\left[\frac{3}{16\pi}\right]^{1/3} a=0.3908a \ . \tag{3}$$

Let us first consider the $PtFe_3$ case. The combinatorial factor in the expression[33] for $|S_{t,2}^{t,2}|^2$ equals 7000, and the single Pt atom in the unit cell has six nearest neighbors (NN's) of the same kind in the distance a. Hence,

$$|S_{\mathrm{Pt},2}^{\mathrm{Pt},2}|^2 \cong 7000(6)(0.3908)^{10} \cong 3.5 \ . \tag{4}$$

Similarly, for $|S_{\mathrm{Fe},2}^{\mathrm{Fe},2}|^2$, we get

$$|S_{\mathrm{Fe},2}^{\mathrm{Fe},2}|^2 \cong 7000(3)(8)(0.3908\sqrt{2})^{10} \simeq 447 \tag{5}$$

for three atoms per unit cell with eight NN's each. The $|S_{\mathrm{Fe},2}^{\mathrm{Pt},2}|^2$ is the same as the second moment of the $l=2$ band in the fcc lattice:

$$|S_{\mathrm{Fe},2}^{\mathrm{Pt},2}|^2 \cong 7000(12)(0.3908\sqrt{2})^{10} \cong 223 \ . \tag{6}$$

The unhybridized bandwidth is now given by

$$W_{\mathrm{Pt},2}=(\tfrac{12}{5}3.5)^{1/2}\Delta_{\mathrm{Pt},2}=2.9\Delta_{\mathrm{Pt},2} \tag{7}$$

and

$$W_{\mathrm{Fe},2}=\left[\frac{12}{(3)(5)}447\right]^{1/2}\Delta_{\mathrm{Fe},2}=19\Delta_{\mathrm{Fe},2} \ . \tag{8}$$

In order to obtain an expression for the unhybridized bandwidth in the elemental fcc metal, one could either use Eqs. (6) and (7), getting

$$W_{M,2}=(\tfrac{12}{5}223)^{1/2}\Delta_{M,2}=23\Delta_{M,2} \tag{9}$$

or, alternatively, calculate $|S_{\mathrm{sc},2}|^2$ for simple cubic lattice,

$$|S_{\mathrm{sc},2}|^2 \cong 7000(4)(12)(0.3908\sqrt{2})^{10} \cong 892 \ , \tag{10}$$

and recover Eq. (9) by

$$W_{M,2}=\left[\frac{12}{(4)(5)}892\right]^{1/2}\Delta_{M,2}=23\Delta_{M,2} \ . \tag{11}$$

The above formulas can be applied to the case of Pt_3Fe by a trivial exchange of Pt and Fe. For a Pt_2Fe_2 structure (AuCu I), the expression for $|S_{\mathrm{Pt},2}^{\mathrm{Pt},2}|^2=|S_{\mathrm{Fe},2}^{\mathrm{Fe},2}|^2$ reads

$$|S_{t,2}^{t,2}|^2 \cong 7000(2)(4)(0.3908\sqrt{2})^{10} \cong 149 \tag{12}$$

and

$$W_{t,2}=\left[\frac{12}{(2)(5)}149\right]^{1/2}\Delta_{t,2}=13,4\Delta_{t,2} \ . \tag{13}$$

To illustrate the accuracy of the above expressions, let us consider the example of fcc Fe at $S_{\mathrm{WS}}=2.68$ a.u. (Table I). With the effective mass $\mu_d=10.12$, the estimated unhybridized bandwidth is 318 mRy as compared with the self-consistently calculated $A-B=332$ mRy. The error is of the order of 5%.

For $PtFe_3$, the values of W are 96 mRy and 227 mRy for Pt and Fe, respectively. They give an estimate of the unhybridized bandwidth. For elements Fe, only *sp-d* hybridization was neglected. For a compound, W gives an estimate of the bandwidth in a lattice with all atoms of different kinds substituted by a vacancy. In a symmetrical case, i.e., in the case when the influence of Pt atoms on Fe bandwidth and *vice versa* are similar, we would expect the ratio $\eta=(A-B)/W$ to be equal to the ratio of coefficients of the Δ parameter as given by Eqs. (7)–(9) and (13) (shown as $\bar{\eta}$ in Table I). We see that η and $\bar{\eta}$ are of the same order of magnitude indeed, but there is a distinct asymmetry: presence of a Pt atom widens the Fe band more than presence of an Fe atom would do, and the opposite is true for the Pt bands. With the ratio of $\bar{\eta}$ instead of η, the Fe band in $PtFe_3$ would have precisely the bandwidth reported in Table I for fcc Fe. Thus, the data in Table I are consistent and quantify the notion concerning the influence of the large Pt 5*d* shell on the Fe bandwidth explained earlier. It will be shown below that the trend found here for $PtFe_3$ holds for all other alloy compositions.

Taking the Stoner parameter I from the exchange splitting of the band centers of Fe *d* bands in the spin-polarized calculations for $PtFe_3$ ($I \cong 67$ mRy$=0.91$ eV), we find that the Stoner criterion [$Ig(E_f)>1$] becomes satisfied for $PtFe_3$ at $S_{\mathrm{WS}} \cong 2.62$ a.u. We conclude, therefore, that the increased lattice constant, *per se*, is not responsible for magnetic instability of this compound. At this lattice constant, the fcc Fe is nonmagnetic,[26] as it is for $S_{\mathrm{WS}}=2.66$ a.u., the equilibrium lattice constant of the NM phase of $PtFe_3$. In the absence of strong covalency effects, the ferromagnetic instability in $PtFe_3$ is due to the presence of the hybridization-induced maximum in the DOS just at the Fermi energy. Nevertheless, while this interpretation holds for $PtFe_3$, for higher Pt concentrations, the Fe *d* band narrowing at $S_{\mathrm{WS}}^{\mathrm{eq}}$ relative to the equilibrium fcc Fe *d* band bandwidth is more significant, and the large lattice constant alone might be responsible for the magnetic instability. A microscopic mechanism leading to such a situation will be discussed in Sec. III C. Further, we will argue that even for $PtFe_3$, the large lattice constant is responsible for its magnetic homogeneity.[5]

From the position of the Fermi level just as at a DOS maximum, one can predict a particular type of the magnetism onset in $PtFe_3$. Following the analysis presented by Moruzzi and Marcus,[34] we expect a second-order transition, i.e., a singular but continuous appearance of magnetic moment at S_{WS} approximately equal to 2.62 a.u. It implies that, if a LS phase[35] exists for this material, it will have a nonzero magnetic moment, in agreement with the recent high-pressure Mössbauer experiment[25] and with our fixed-spin-moment[36] (FSM) calculations.[28]

The analysis of the bandwidth based on the canonical band theory could, in principle, be extended to an analysis of hybridization strength. Andersen *et al.*[32] gave the expressions that allow for such an estimate by calculating either the hybridization-induced band mass-center shift or the number of the tl electrons in the $t'l'$ band. The validity of these expressions is, however, limited to the case of weak hybridization, and they fail utterly when

applied to $PtFe_3$. This indicates that in spite of the existence of almost separated Pt and Fe subbands, hybridization cannot be considered weak for the Pt-Fe system.

B. Ferromagnetic $PtFe_3$

The electronic structure of the ferromagnetic phase of $PtFe_3$ along the symmetry lines of the simple cubic lattice is shown in Figs. 2 and 3 for the majority and minority spins, respectively. In Table II the self-consistent potential parameters are listed, from which the band structure and the density of states can be recovered by means of the standard LMTO precedure.[23] The spin-polarized DOS is shown in Fig. 4(a). In agreement with experiment, there is a stable ferromagnetic phase with the equilibrium S_{WS} equal to 2.726 a.u. An interesting feature of the band structure of $PtFe_3$ is two flat bands along the $\Delta(\Gamma$-$X)$ direction, for the majority spins bracketing the Fermi level (Fig. 2). Carbone *et al.*[35(b)] found these two bands just below E_F split by ~ 0.7 eV. The calculated splitting is ~ 0.5 eV, and the bands are some 0.25 eV too high with respect to E_F. This is because they are calculated for the theoretical equilibrium lattice constant, which is $\sim 1.5\%$ smaller than the experimental one. Moreover, the measurements have been performed for a nonstoichiometric sample $Pt_{28}Fe_{72}$. The calculations carried out for $S_{WS}=2.77$ a.u. ($a=3.75$ Å) place both flat bands at positions found in experiment.[35(b)] However, the band structure of Fig. 2 has been quoted in Ref. 7 [Fig. 14(d)] as an example of the LS phase. This is not entirely correct, since the loss of magnetic moment caused by the shift of the upper bound above E_F is only $\sim 0.15\mu_B$.

The only other calculation of the electronic structure

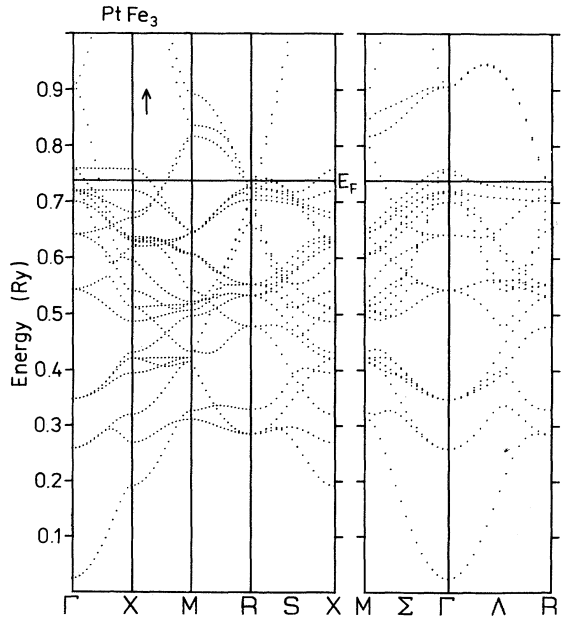

FIG. 2. Band structure for majority spins in ordered ferromagnetic $PtFe_3$, along symmetry lines of the sc Brillouin zone.

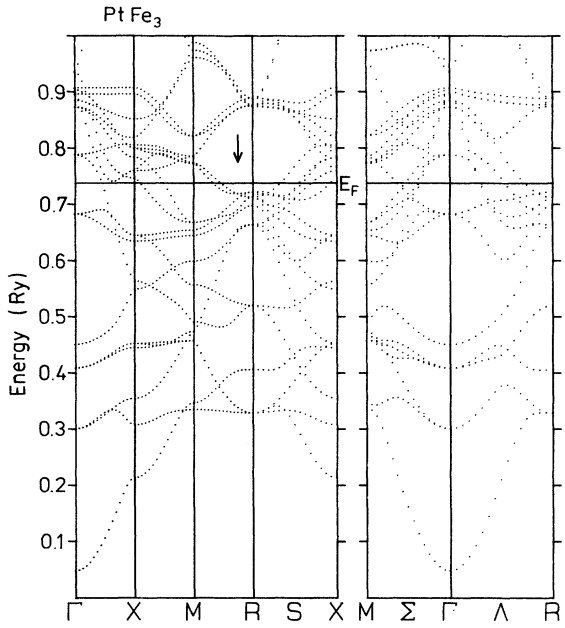

FIG. 3. Band structure for minority spins in ordered ferromagnetic $PtFe_3$ along symmetry lines of the sc Brillouin zone.

of $PtFe_3$ has been reported by Hasegawa.[19] He used the self-consistent augmented plane-wave (APW) method with muffin-tin potential and carried out the calculation for $S_{WS}=2.77$ a.u. There is an overall fair agreement with our results at the same lattice constant. The magnetic moments of Fe differ a little ($2.5\mu_B$ in Ref. 19 and $2.66\mu_B$ in the present work), but Hasegawa's Pt moment ($0.5\mu_B$) is much larger than ours ($0.3\mu_B$). This difference can probably be attributed to different potential shapes:

TABLE II. LMTO potential parameters for the ferromagnetic $PtFe_3$ at equilibrium lattice constant: $S_{WS}=2.7247$ a.u., $S_{Pt}=2.8893$ a.u., and $S_{Fe}=2.6652$ a.u.

		Pt		Fe	
		↑	↓	↑	↓
E_ν(Ry)	s	0.280	0.318	0.302	0.347
	p	0.484	0.564	0.446	0.502
	d	0.469	0.452	0.570	0.614
$\omega_\nu(-)$(Ry)	s	0.007	−0.034	0.194	0.196
	p	0.932	0.844	1.069	1.064
	d	0.023	0.054	0.020	0.150
$S\Phi^2(-)$(Ry)	s	0.302	0.303	0.371	0.379
	p	0.315	0.313	0.345	0.350
	d	0.046	0.047	0.027	0.035
Φ_-/Φ_+	s	0.850	0.848	0.860	0.861
	p	0.707	0.701	0.692	0.695
	d	0.106	0.120	−0.020	0.045
$\langle\dot{\phi}_\nu^2\rangle^{1/2}$(Ry^{-1})	s	0.252	0.254	0.199	0.194
	p	0.160	0.163	0.152	0.151
	d	0.897	0.850	1.299	1.101

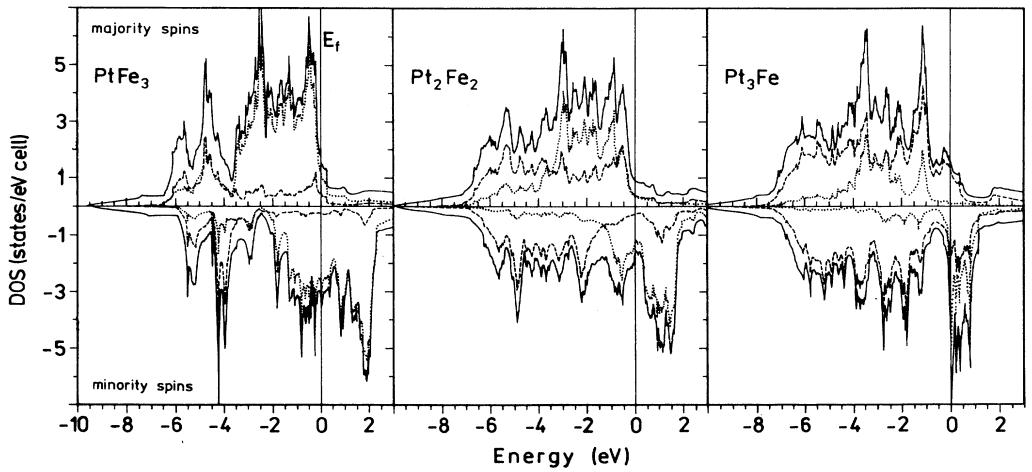

FIG. 4. Spin-resolved total and d-projected densities of states for ferromagnetic phases of $PtFe_3$, Pt_2Fe_2, and Pt_3Fe, calculated at equilibrium lattice constants.

the pure d moment on Pt in our calculations is $0.44\mu_B$, and we observe a relatively large negative contribution from p ($-0.09\mu_B$) and s ($-0.04\mu_B$) electrons, which, in Hasegawa's calculation, might be ascribed to the interstitial region. Further, the Fe d exchange band splitting is 0.2 Ry in Ref 19 and 0.18 in our calculation estimated from the band-center splitting, see Table III. Finally, the DOS at Fermi level is 59 and 62 states/Ry cell in Ref. 19 and in our calculation, respectively. Our value corresponds to the linear coefficient in the specific heat $\gamma = 10.8$ mJ/mol K^2, in a reasonable agreement with the experimental value[5] of 9.6 mJ/mol K^2. We should also mention a general agreement of the total state densities (Fig. 5) except for the energy scale in Fig. 9 of Ref. 19, which is not in eV as indicated but probably in the units of 2 ev.

TABLE III. d bands parameters for the Pt-Fe system equilibrium lattice constants. Data for fcc Fe correspond to $S_{WS}=2.68$ a.u. All values are given in Ry. Δ is the bandwidth $[12.5S\Phi^2(-)]$, E is the center of the occupied part of the band, C is the mass center of the band, $\omega \cong C-E$, and E_F is the Fermi energy (Ry). $\uparrow$ and $\downarrow$ refer to majority and minority bands, respectively.

	Fe					
	LS	HS	$PtFe_3$	Pt_2Fe_2	Pt_3Fe	Pt
$Fe\Delta_v^{\uparrow}$	0.332	0.327	0.337	0.318	0.294	
	0.381	0.424	0.426	0.415	0.399	
$E_v^{\uparrow}$	−0.205	−0.200	−0.200	−0.228	−0.305	
	−0.181	−0.157	−0.154	−0.177	−0.234	
$C_v^{\uparrow}$	−0.167	−0.182	−0.181	−0.216	−0.302	
	−0.076	−0.012	−0.010	−0.030	−0.083	
$\omega_v^{\uparrow}$	0.038	0.017	0.019	0.012	0.003	
	0.106	0.150	0.147	0.151	0.156	
$Pt\Delta_v^{\uparrow}$			0.574	0.551	0.524	0.504
			0.576	0.556	0.534	
$E_v^{\uparrow}$			−0.303	−0.295	−0.321	−0.325
			−0.325	−0.315	−0.329	
$C_v^{\uparrow}$			−0.280	−0.274	−0.304	−0.304
			−0.276	−0.268	−0.289	
$\omega_v^{\uparrow}$			0.023	0.021	0.019	0.021
			0.048	0.046	0.040	
E_F	−0.059	−0.046	−0.038	−0.047	−0.073	−0.105

C. Ferromagnetic Pt_2Fe_2 and Pt_3Fe

The spin-resolved and total DOS for all calculated FM phases at equilibrium lattice constants are plotted in Figs. 4 and 5, respectively. In Tables III and IV the relevant band parameters and occupation numbers are listed. Also, in both tables, the data for HS and LS phases of fcc Fe (Ref. 37) at $S_{WS}=2.68$ a.u. and for fcc Pt are included for comparison. Before discussing the general trends in the Pt-Fe system, we want to return briefly to the $PtFe_3$ phase. A comparison of the data in Tables III and IV for Fe and $PtFe_3$ at equilibrium lattice constant and for the HS phase of fcc Fe at $S_{WS}=2.68$ a.u. shows that the band parameters and the partial charges are *almost identical* for these cases. Also, the magnetic moments are very close. Now, the $S_{WS}=2.68$ a.u. is a "magic" value for fcc Fe at which the multiple magnetic phases coexist.[26-28] It is, therefore, justified to expect that also $PtFe_3$ will display a kind of metamagnetic behavior and a magneto-volume instability. This has been confirmed by model calculations[28] and, recently, by a full-scale FSM study.[38] It is noteworthy, that the Fe band parameters and partial charges calculated for ordered $Ni_{0.375}Fe_{0.625}$ are also very close to the values discussed above.[30,29] In all three cases (fcc Fe at $S_{WS}=2.68$ a.u., $PtFe_3$, and $Ni_{0.375}Fe_{0.625}$); the Fermi level is situated at the edge of the first maximum of the majority-spin DOS. The observed correlation supports the hypotheses formulated by Williams *et al.*[15] that the Invar materials are metamagnetic, although an explicit correlation between a particular type of metamagnetism and the Invar behavior remains yet to be established. On the other hand, the firm statement of Williams *et al.*[15] that there is no connection between weak ferromagnetism and the Invar problem appears to be doubtful, since the metamagnetic behavior of Invar materials seems to be directly correlated with the transition from strong to weak ferromagnetism.

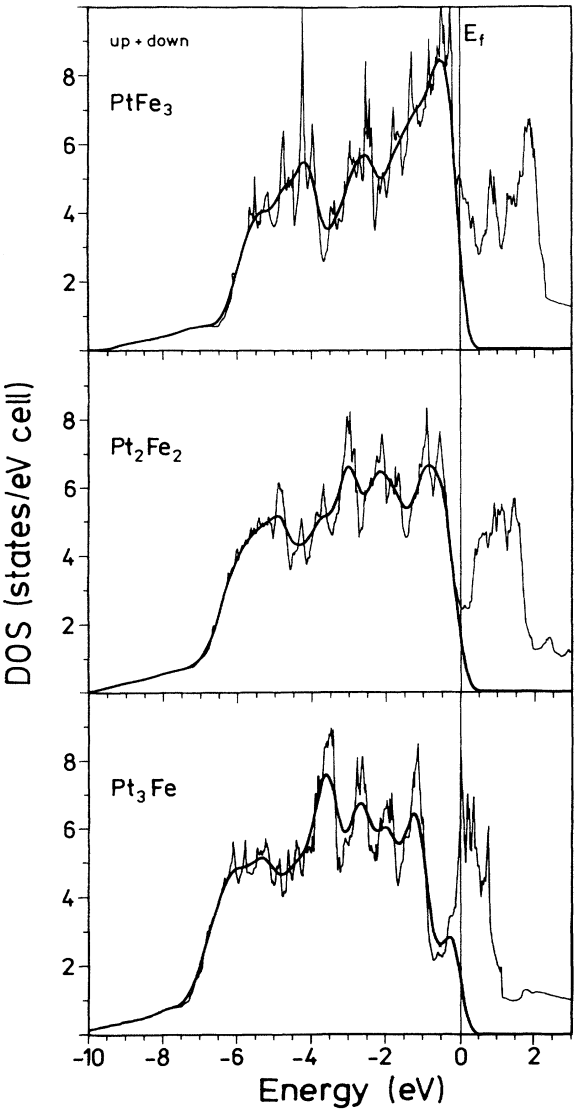

FIG. 5. Total densities of states for ferromagnetic phases of $PtFe_3$, Pt_2Fe_2, and Pt_3Fe, calculated at equilibrium lattice constants. The bold line shows the convolution of the occupied part of the spectrum with the Gauss function ($\sigma=0.3$ eV).

Let us now focus on some general trends in the electronic structure of the Pt-Fe system. First, we note that the Fermi level is swept across the spin-up–spin-down valley of the DOS with growing Pt concentration. The calculations predict that the value of the DOS at the Fermi level will strongly depend on composition for the Pt-Fe system. The calculated values of the DOS (E_F) and the corresponding linear coefficients in the specific heat γ are 68.0, 34.8, and 82.0 states/Ry unit cell) for FM $PtFe_3$, Pt_2Fe_2, and Pt_3Fe, respectively, with the corresponding γ coefficients (in mJ/mol K^2) of 11.8, 6.04, and 14.2. Secondly, Fig. 4 expressively demonstrates that the rigid-band model is not applicable—the shape of the partial state densities varies strongly with composition. However, the sweep of the Fermi level across the spin-up–spin-down valley in the total DOS upon composition change deceptively awakens memories of this somewhat discredited model.[39] Indeed, it is tempting to argue that the growing electron count pushes the Fermi level upward. This is as false as the conviction that the rigid-band model is a necessary prerequisite for an explanation of the Slater-Pauling curve. From the data in Table IV, we note that the total number of the majority electrons per atom $\bar{N}_\uparrow$ remains almost constant, in spite of composition change (with a slight tendency to decrease for $PtFe_3$), and equals ≈ 5.30. For the HS phase of the fcc Fe $\bar{N}_\uparrow=5.25$. As pointed out by Malozemoff, Williams, and Moruzzi,[40] and Kübler,[41] a constancy of either $\bar{N}_\uparrow$ or $\bar{N}_\downarrow$ is, essentially, the reason that the net magnetic moment follows the Slater-Pauling curve. As long as a material is magnetically strong, the Fermi level remains above the leading maximum of the majority DOS, and $\bar{N}_\uparrow$ remains equal to ≈ 5.3. This number consists of five *d* electrons and ≈ 0.3 *sp* electrons hybridized with the *d* band, the constant number of the *sp* electrons being warranted by the presence of the gap in the *sp* DOS above

the d DOS maximum.[40,42] As long as $\bar{N}_\uparrow$ is equal to this constant, the net moment follows the branch of the Slater-Pauling curve described by

$$\bar{M}=2\bar{N}_\uparrow-\bar{Z}=10.6-\bar{Z}\ , \tag{14}$$

where $\bar{Z}$ denotes the average valency. As shown in Fig. 6, the $\bar{M}$ for Pt-Fe system follows this line quite accurately. The missing 0.07 electrons for $PtFe_3$ indicate a beginning of magnetic weakness in the system. Equation (14) is a correct one, in contrast to the rigid-band expression $\bar{M}=xM_A+(1-x)M_B$, where M_A and M_B are constant, composition-independent magnetic moments of alloy constituents. This expression, while reproducing the experimental data quite well, has little physical content. Applying it to $PtFe_3$, one would be forced to take $M_{Fe}=2.6\mu_B$ and an *ad hoc* value $M_{Pt}=0.6\mu_B$. In reality, the local magnetic moments in the Pt-Fe system strongly depend on alloy composition: the Fe moment increases rapidly from $2.54\mu_B$ in $PtFe_3$ through $2.84\mu_B$ in Pt_2Fe_2 to $3.28\mu_B$ in FM Pt_3Fe. The behavior of the Pt-Fe system is a very good example of the theory of Malozemoff, Williams, and Moruzzi.[40]

As we have mentioned before, the ratio of the atomic radii was kept constant throughout the calculations. Therefore, the calculated *changes* in the charge transfer from Fe to Pt are physically meaningful. We observe that

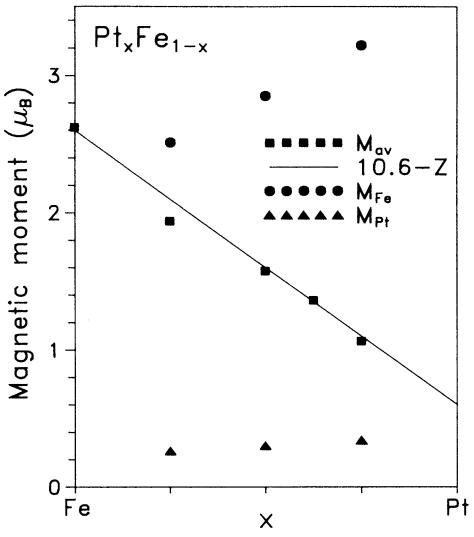

FIG. 6. Composition dependence of the calculated average- and local-magnetic moments for the ferromagnetic ordered phases of the $Pt_{1-x}Fe_x$ alloy.

TABLE IV. LMTO occupation numbers for the Pt-Fe system at equilibrium lattice constants. Data for fcc Fe correspond to $S_{WS}=2.68$ a.u. $\bar{N}$ denotes the total number of electrons of either spin per atom and Δq the charge transfer. ↑ and ↓ refer to the majority and minority electrons, respectively.

	Fe					
	LS	HS	$PtFe_3$	Pt_2Fe_2	Pt_3Fe	Pt
Fe s ↑	0.32	0.32	0.30	0.29	0.29	
↓	0.33	0.34	0.31	0.29	0.27	
p ↑	0.38	0.38	0.38	0.37	0.36	
↓	0.42	0.44	0.39	0.37	0.34	
d ↑	3.96	4.55	4.56	4.69	4.83	
↓	2.57	1.97	2.00	1.85	1.59	
Total ↑	4.70	5.25	5.24	5.35	5.48	
↓	3.30	2.75	2.70	2.51	2.20	
Pt s ↑			0.43	0.41	0.40	0.76
↓			0.47	0.44	0.40	
p ↑			0.44	0.43	0.42	0.83
↓			0.52	0.50	0.45	
d ↑			4.32	4.35	4.40	8.41
↓			3.99	4.00	4.03	
Total ↑			5.19	5.19	5.22	10.00
↓			4.98	4.94	4.88	
$\bar{N}$ ↑	4.70	5.25	5.23	5.27	5.29	
$\bar{N}$ ↓	3.30	2.75	3.27	3.73	4.21	
Δq Fe			−0.057	−0.130	−0.320	
Δq Pt			0.172	0.130	0.107	

the charge transfer from Fe to Pt increases with growing Pt concentration, being equal to -0.06 electrons per Fe atom for $PtFe_3$ and -0.32 electrons per Fe atom for Pt_3Fe. As can be seen from Table III, this charge transfer, together with increasing lattice constant, causes a lowering and narrowing of the Fe $3d$ bands for both spin directions. The distance between the Fermi level and the majority-spin-band upper edge increases slightly, and so does the number of Fe $N_\uparrow$ electrons, which goes up from $PtFe_3$ to Pt_3Fe by 0.24. Hence, the electrons lost by Fe must be drawn from the minority band, and there must be $0.24+0.26=0.5$ electrons less there. Since there are 0.24 extra electrons in the Fe majority band, the Fe magnetic moment increases by $0.74\mu_B$, from 2.54 to $3.28\mu_B$. This evolution of the Pt-Fe bands with composition is schematically illustrated in Fig. 7, and it explains the sweep of the Fermi level across the spin-up–spin-down valley of DOS. An alternative interpretation can be associated with this figure: due to lowering of the Fe d states with growing Pt concentration, the band centers for Fe $3d_\uparrow$ and Pt $5d$ band coincide for Pt_3Fe. This is analogous to the situation reported for FeCo by Schwarz *et al.*[31] The picture is not as obvious as in the case of FeCo (Ref. 31) due to large differences in the bandwidths of constituent atoms in the Pt-Fe system, a complication not present for FeCo compound. However, a careful analysis of Fig. 4 shows that for the FM phase of $PtFe_3$ one can still distinguish, as for the NM phase, the Fe and Pt subbands, and a comparison with the FM fcc Fe bands reveals no amplitude enhancement of the Fe $d_\downarrow$ DOS in the upper part of the spectrum. For Pt_3Fe, the Pt and Fe DOS is evenly distributed over the energy range of the majority states, forming a truly common band. (It is remarkable that a truly common band for the majority electrons is found not for the itinerant $PtFe_3$ but for being close to the local limit Pt_3Fe.) For minority states, a redistribution of spectral weights typical for covalency effect can be observed and, thereby, a moment enhancement. This demonstrates consistency of our analysis.

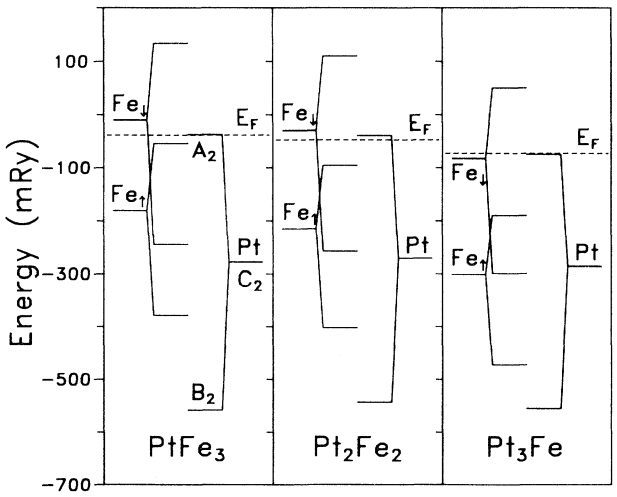

FIG. 7. Schematic picture of the evolution of band widths and band centers shifts with composition for ordered ferromagnetic phases of the Pt-Fe alloy.

A reason for the observed charge transfer is the electronegativity difference of Pt and Fe. This difference can be easily calculated. According to Mulliken,[43] the electronegativity χ can be written as

$$\chi=\tfrac{1}{2}(I+A)\,, \tag{15}$$

where I denotes the ionization potential and A denotes the electron affinity. The electron removal energies can be expressed in the local-density approximation by eigenvalues calculated at one-half occupancy (the transition state concept of Slater[44]). Hence, for Pt with its ground state $[Xe]4f^{14}5d^{10}6s^0$, the ionization potential I is given by the eigenvalue $\varepsilon^{5d}_{n=9.5}$, and the electron affinity A is given by $\varepsilon^{6s}_{n=0.5}$. For Fe, the atomic ground state is $[Ne]3d^64s^2$, and I and A are given by $\varepsilon^{4s_\downarrow}_{n=0.5}$ and $\varepsilon^{4p}_{n=0.5}$, respectively. We have calculated these values using the atomic program[45] used to generate the core charge densities, with the same exchange-correlation potential as in the crystal calculations. The results are, for Pt, $I=-8.38$ eV, $A=-1.66$ eV, and $\chi=-5.02$ eV, and, for Fe, $I=-7.56$ eV, $A\cong 0$, and $\chi=-3.78$ eV. We see, therefore, that the higher Pt electronegativity results not as much from the higher binding energy of the d electrons but, rather, from the higher electron affinity that, in turn, is mainly caused by the scalar relativistic corrections acting strongly on $6s$ electrons. We conclude, therefore, that the moment-enhancing mechanism in the Pt-Fe system with growing Pt concentration is primarily caused by scalar relativistic effects that lower the $6s$ states of Pt.

Kulikov, Kalatov, and Yakchimovich[19(b)] calculated the nonmagnetic band structure of Pt_3Fe using a mutation of the Korringa-Kohn-Rostoker (KKR) method with the muffin-tin potential and S_{Pt}/S_{Fe} ratio $\cong 1.1$. They report a charge transfer of $\Delta q=0.22$ from Pt to Fe. This is in obvious disagreement with our results and with the electronegativity argument. We suspect that this discrepancy is due to neglect of the scalar relativistic terms in the calculations of Kulikov, Kalatov, and Yakchimovich.[19(b)]

In Table V, we present the bandwidth analysis for all ferromagnetic phases. The quantities listed were discussed in Sec. III A. In agreement with the previous discussion, we observe a systematic growth of the band masses with growing Pt content. The characteristic asymmetry is quite distinct for all phases, as mentioned in Sec. III A. According to the discussion therein, we recognize as a general feature of the electronic structure of the Pt-Fe system the following.

(a) The Fe bandwidth is always larger than it would be in fcc Fe at a corresponding lattice constant, and the opposite is true for the Pt bandwidth as compared with fcc Pt. Evidently, a reason for this is connected with the mutual relationship of the Pt and Fe atomic radii and the alloy lattice constant. In particular, we expect a reverse behavior for the Ni-Fe system, since the atomic radius of Ni is smaller than that of Fe.

(b) The influence of Pt atoms on the Fe bandwidth and

TABLE V. The bandwidths (in mRy) of Pt and Fe spin-polarized d bands in the ordered ferromagnetic phases of the Pt-Fe system at the equilibrium lattice constants. μ is the effective mass in units of m_0, W is the estimate based on the canonical band theory [Eqs. (7), (8) and (13)], A-B is the self-consistently calculated bandwidth, η is the $(A\text{-}B)/W$, and η is the ideal ratio (see text).

Band		μ	W	A-B	η	$\bar{\eta}$
		$PtFe_3$, FM, $S_{WS}=2.725$ a.u.				
Pt	↑	5.18	90	528	5.81	7.93
	↓	5.09	93	539	5.79	
Fe	↑	10.32	228	328	1.44	1.21
	↓	8.77	266	388	1.46	
		Pt_2Fe_2, FM, $S_{WS}=2.8115$ a.u.				
Pt	↑	5.33	362	500	1.38	
	↓	5.24	362	511	1.41	1.72
Fe	↑	10.84	134	305	2.28	
	↓	8.89	161	370	2.30	
		Pt_3Fe, FM, $S_{WS}=2.888$ a.u.				
Pt	↑	5.45	437	486	1.11	1.21
	↓	5.37	456	492	1.08	
Fe	↑	11.35	25	288	11.52	7.93
	↓	9.24	31	354	11.42	

the influence of Fe atoms on the Pt bandwidth are comparable, although of different signs, the former being a little stronger.

The data in Table V illustrate yet another aspect of magnetic interactions in the Pt-Fe system. For $PtFe_3$, the Fe bandwidth is mostly ($\sim 70\%$) due to the direct Fe-Fe interaction. For Pt_2Fe_2, this interaction accounts for only 40% and, for Pt_3Fe, for less than 10% of the total bandwidth. This suggests that, while for $PtFe_3$ the direct exchange dominates, for Pt_3Fe the Fe-Fe magnetic interactions are mediated by Pt $5d$ shell. In this sense, Pt_3Fe is similar to Heusler alloys where there is no significant direct interaction among the d states of different Mn atoms.[15]

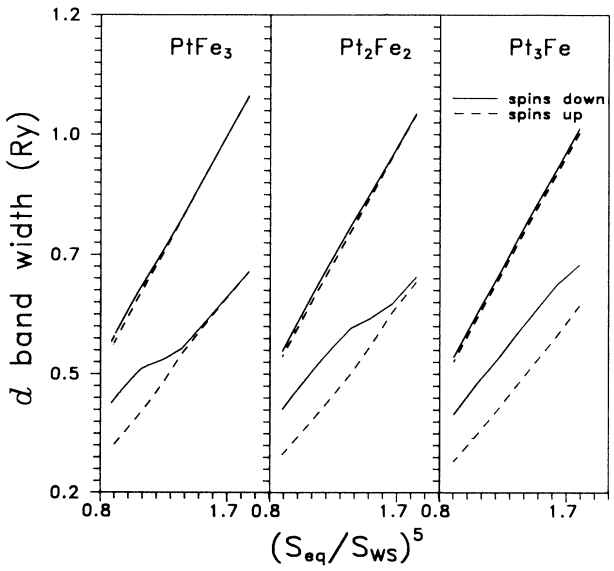

FIG. 8. Band widths of the Pt and Fe d bands (as given by $12.5 \cdot S\Phi^2$) vs $(S_{eq}/S)^5$ for ordered ferromagnetic phases of the Pt-Fe alloy.

We close this part of our presentation with Fig. 8, where the d bandwidth for both atoms is plotted as a function of $(S_{WS}/S_{eq})^{-5}$. According to Heine's r^{-5} rule one expects the d bandwidth to follow a straight line in such a coordinate system. We see that this holds very well for Pt d bandwidth, but a breakdown of magnetism caused by lattice contraction introduces a disturbance for the Fe d bands. We also note a characteristic feature that, according to our experience, is typical for $3d$ transition metals and their compounds: at the onset of magnetism, the minority d band widens, whereas the bandwidth of the majority band decreases only a little, so that the values of the up and down bandwidths do not symmetrically bracket the nonmagnetic bandwidth.

D. Magnetic moments

Since the paper of Nakamura, Sumiyama, and Shiga,[5] it is commonly believed that $PtFe_3$ is a strong ferromagnet. This conviction is based mainly on the linear dependence of the average magnetic moment on composition, without a trace of any anomaly, and on the composition dependence of the hyperfine field. On the other hand, the large value of the high-field susceptibility of Pt-Fe Invar, comparable with that of Fe-Ni alloys,[10] contradicts this simple picture. Further doubts have been raised by Oomi and Mori,[46] who pointed out that the anomalously large difference between the paramagnetic and ferromagnetic bulk modulus at high temperatures makes it doubtful to regard $PtFe_3$ as strong ferromagnet, at least at high temperatures. In Fig. 9, we show the calculated volume dependence of the Fe and average magnetic moment for all FM phases. The normalized plot (right-hand panel) clearly demonstrates how imprecise is the common definition of strong magnetism. Indeed, there are almost no holes either in the majority band of $PtFe_3$ or in the majority bands of other FM phases. On the other hand, the volume dependence of the local and average magnetic moments is very different, ranging from an indestructible moment of Pt_3Fe to a very soft one for $PtFe_3$. This is obviously correlated with a position of the Fermi level with respect to the leading peak of the majority DOS, as discussed in Sec. III C. The pressure derivatives of the net and local-magnetic moments at equilibrium, $\partial \ln \bar{M}/\partial p|_{M_0}$ are listed in Table VI. For $PtFe_3$, the calculated value equals -7.6×10^{-4} kbar^{-1} and compares well with the experimental value[47] of -7×10^{-4} kbar^{-1} estimated from magnetization measurements at 4.2 K. This gratifying agreement supports the conclusion about a homogeneous magnetic ground state of $PtFe_3$. Further, our observations reconcile an apparent disagreement between the susceptibility measurements and other experimental indications. Although we did not explicitly calcu-

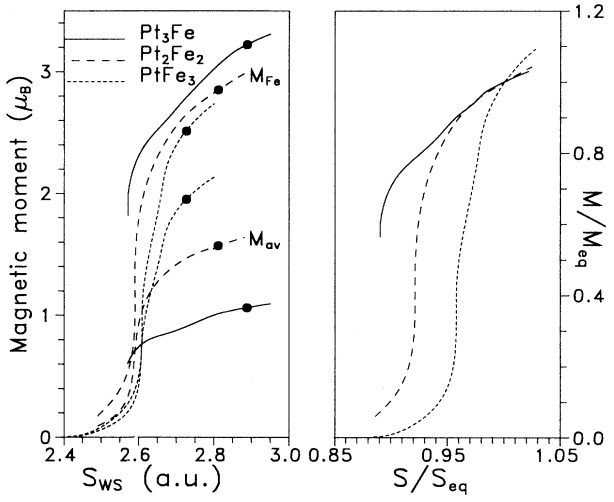

FIG. 9. Volume dependence (as represented by the average Wigner-Seitz radius) of the average and Fe local magnetic moments for the ferromagnetic ordered phases of the Pt-Fe alloy (left hand, panel, heavy dots indicate the equilibrium values). Right-hand panel displays the normalized plot of M/M_{eq} vs S/S_{eq}. Note the different behavior of $PtFe_3$ as compared with Pt_2Fe_2 and Pt_3Fe.

late the high-field susceptibility, it is obvious that it will be much larger for $PtFe_3$ than for the phases with almost saturated moment. Given the similarity of the $PtFe_3$ and $Ni_{0.375}Fe_{0.626}$ electronic structure,[30] there is no reason to expect very different high-field susceptiblities for these substances. Concluding this paragraph, we are inclined to describe $PtFe_3$ as an "almost strong ferromagnet," in order to underline a different volume and pressure dependence of its local and average magnetic moment in comparison with very strong ferromagnetic phases with a higher Pt content.

From the foregoing discussion of the moment-enhancing mechanisms and from the data in Tables III, V, and VI, where the bandwidths and the magnetic moments are listed, one might gain a feeling of a very simple relation between the two: a larger moment corresponds to a smaller bandwidth and *vice versa*. Actually, this simple correspondence holds only for the electronic structures at equilibrium. Figure 9 and the preceding discussion of Pt influence on the Fe d bandwidth show that this simple relation generally cannot be valid. From Fig. 9, we realize that for a given lattice constant, the local Fe moments increase with the Pt concentration. Taking $S_{WS}=2.80$ a.u. as an example, we get the Fe magnetic moments of 2.74, 2.83, and $3.00\mu_B$ for $PtFe_3$, Pt_2Fe_2, and Pt_3Fe, respectively. On the other hand, if our discussion of the bandwidths in the Pt-Fe system was correct, we expect an increase of the Fe d bandwidth for these sequences. Indeed, the Fe $d_\uparrow$ band mass decreases and takes the values of 11.3, 10.7, and 10.0, corresponding to $\sim 20\%$ bandwidth increase of the Fe $d_\uparrow$ states from $PtFe_3$ to Pt_3Fe. However, an analogous situation has already been recognized for a much simpler system. We have shown[37] that for fcc Fe the HS phase is more itinerant that the LS one. Similarly, as for fcc Fe, this apparent paradox can be explained by the notion of Williams *et al.*[15] that a localized magnetic moment in itinerant systems does not result from the localization of any occupied states but, rather, from the exclusion of the minority-spin electrons from some localized volume in the interior of a magnetic atom.

The $M(S_{WS})$ curves (Fig. 9) should not be taken too seriously for large lattice compressions. In this region, spin-polarized calculations do not converge well, and the resulting magnetic moment depends on the initial conditions. The results of Bagayako and Callaway[48] for fcc Fe evidently suffer from the same difficulties: instead, to indicate the HS and LS phases,[26–28] their $M(S_{WS})$ curve just interpolates between them. These difficulties are caused by a very small total energy difference between different magnetic phases at small atomic volumes. $PtFe_3$ possess a LS phase with a rather small magnetic moment.[28] The energy difference between this and the nonmagnetic phase[38] is negligible, i.e., the electrons can flow

TABLE VI. Ground-state properties of the Pt-Fe system: equilibrium Wigner-Seitz radii S_{eq} (a.u.), bulk moduli B (Mbar), linear coefficients of the Murnaghan equation of state $b \equiv dB/dp$, local and average magnetic moments M (μ_B) and their pressure derivatives $d\ln M/dp$ (GPa^{-1}).

	$PtFe_3$ NM	$PtFe_3$ FM	Pt_2Fe_2 FM	Pt_3Fe FM	Pt_3Fe AF
S_{eq}	2.654	2.726	2.811	2.888	2.904
B	3.19	1.96	2.47	2.62	2.56
b	5.07	2.91	5.33	5.66	3.71
M_{av}		1.95	1.57	1.06	0.0
M_{Fe}		2.51	2.85	3.22	3.43
M_{Pt}		0.26	0.30	0.34	0.17/0.0
$d\ln M/dp$					
M_{av}		-7.62×10^{-3}	-2.42×10^{-3}	-3.43×10^{-3}	
M_{Fe}		-7.66×10^{-3}	-2.53×10^{-3}	-1.23×10^{-3}	-1.26×10^{-3}
M_{Pt}		-1.26×10^{-2}	-1.85×10^{-3}	-1.06×10^{-2}	

from one to the other spin subsystem at no energy cost. Such phases are only detectable by the FMS method[36,26] of spin-polarized band-structure calculations. It seems that no conventional (floating moment) spin-polarized calculations can be trusted in a region of a magnetic instability.

In order to investigate the influence of local environment on the magnetic moment, we have calculated self-consistently the electronic structure of the ordered Pt_5Fe_3 compound. The supercell has been chosen so that the Fe NN environments in Pt_2Fe_2 and in $PtFe_3$ were represented and a highest possible symmetry retained. Figure 10 shows the assumed structure. There are two unequivalent Fe atom positions: j (0,0,0; $\frac{1}{2},\frac{1}{2},0$) and g (0,0,1), and two Pt positions: i ($0,\frac{1}{2},\frac{1}{2}$; $\frac{1}{2},0,\frac{1}{2}$; $0,\frac{1}{2},1\frac{1}{2}$; $\frac{1}{2},0,1$) and d ($\frac{1}{2},\frac{1}{2},1$), according to the *International Crystallographic Tables*. The space group of this lattice is D^1_{4h}, and the Bravais lattice is simple tetragonal with $c/a=2$. The NN environment of the Fe atoms in positions j is the same as in Pt_2Fe_2 (four Fe and eight Pt NNs). Fe atoms in positions, g have 12 Pt NN's as in $PtFe_3$. Pt atoms in position d have a NN environment as in $PtFe_3$; for position i, there is no analogy. The local moments reported below were calculated for $S_{WS}=2.87$ a.u. For Pt positions, i and g support almost equal moments of $0.33\mu_B$. The Fe moments are $3.08\mu_B$ and $3.31\mu_B$ in positions j and g, respectively. The corresponding moments calculated for Pt_2Fe_2 and $PtFe_3$ are $2.98\mu_B$ and $3.20\mu_B$, respectively. Having explained (Sec. III C) the relationship between the charge transfer and magnetic moment, we can check how it works for Pt_5Fe_3. It is gratifying to note that the Fe charge transfer in the four cases enumerated above is -0.15, -0.29, -0.16, and -0.25, respectively. We also see that, for Pt_5Fe_3, a larger charge transfer corresponds to a larger moment, and that there is a good correlation between the moment and the local environment. A very similar trend has been found for the Ni-Fe system.[30]

Steinbach, Brand, and Keune[49] carried out a Mössbauer study for $Pt_{3-x}Fe_{1-x}$ alloy. They reported on a satellite structure in the Mössbauer spectra of $Pt_{70}Fe_{30}$, indicating a magnetic inhomogeneity of the sample. Apart from the main line, there is an additional maximum in the hyperfine field distribution at a somewhat higher field. The authors interpreted it as arising from the magnetic moment of the Fe atoms in the center of the basal plane in Fig. 10. Our results do not support this interpretation. In our view, an increased number of Fe NN's in the Pt-Fe system always decreases the magnetic moment. It remains, however, a question of whether our result for a coherent structure are directly applicable here. We note that, whereas Steinbach, Brand, and Keune[49] consider the corner and the central atoms of the basal plane as having different environments, this is not the case for our superlattice: all atoms in the basal plane are crystallographically equivalent and different from the atoms in the corners of the intermediate plane. It is also not clear how the authors of Ref. 49 arrived at their theoretical relative intensities of the main line and the satellites. The problem seems to be intriguing and calls for a reexamination.

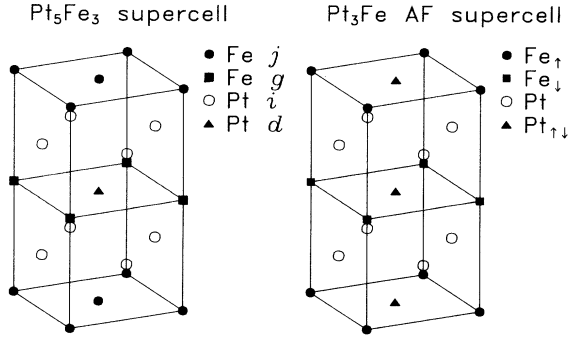

FIG. 10. Supercells used in the calculations for FM Pt_5Fe_3 and AF Pt_3Fe.

E. Antiferromagnetic Pt_3Fe

Below $T_c=100$ K Pt_3Fe is an antiferromagnet of the type I.[50] Since this spin alignment implies a symmetry that is computationally difficult to treat, we have calculated the electronic structure of the compound (Fig. 11) for the supercell shown in Fig. 10. This spin arrangement corresponds rather to the AF III structure. The lattice is simple tetragonal with $c/a=2$, and its space group is D^1_{4h}. A closer look at the lattice reveals that there are two inequivalent positions of Pt atoms in the unit cell: since the Fe spins in the $z=$const planes are ordered ferromagnetically, the Pt atoms centering these planes see all four Fe NNs of the same spin directions. So, we *a priori* expect a nonzero magnetic moment for one-third of the Pt atoms. The calculations were carried out for a few lattice constants. The equilibrium lattice constant for the AF Pt_3Fe phase has been found 0.5% larger as compared with the FM phase. The Fe magnetic moment of $3.46\mu_B$ was found. The Pt moment in $z=$const planes equals $0.17\mu_B$ and couples ferromagnetically to Fe moments. The experimental values[50] for the Fe and Pt moments are 3.3 and $0\mu_B$. The agreement for Fe is rather good. What concerns the Pt moment, is that it is an artifact resulting from the assumed Fe spin alignment. For the AF II structure every Pt atom is surrounded by an equal number of the Fe atoms with magnetic moments of either sign, and one does not expect any Pt moment.

An inspection of the band parameters and their comparison with band parameters of the FM phase reveals a very close resemblance. In particular, the Fe bandwidth does not change. This is a further evidence that there is little direct interaction of Fe d shells in Pt_3Fe. (Such interaction, when present, would lead to band narrowing in the AF phase as compared with the FM phase.) An important question that should be answered now is why the Pt_3Fe is antiferromagnetic. Unfortunately, we do not find a clear-cut answer here, and we must content ourselves with speculations. In a somewhat similar case of the Heusler alloys, Williams *et al.*[15] present an elegant

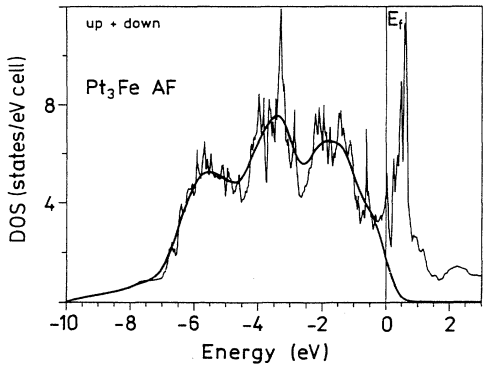

FIG. 11. Density of states for the antiferromagnetic phase of Pt_3Fe at equilibrium lattice constant.

discussion of the competing exchange and covalence effects. They argue that, in the Heusler alloys, the covalent interactions in the antiferromagnetic state cause a loss of the local magnetic moment and of exchange energy, causing the strong preference for the ferromagnetic alignment. This happens despite the fact that covalency effects *per se* favor the antiferromagnetic alignment for the half-filled bands. Now, from the comparison of the FM and AF local Fe moments in Pt_3Fe, we see that, for this compound, the local moment is enhanced for the AF ordering rather than for the FM one. Thus, one could expect that covalence mechanism as a whole will strongly prefer the antiferromagnetic spin alignment. Now, however, one might reverse the problem and ask why the preference for ferromagnetism appears for lower Pt concentrations. Since the direct Fe-Fe interactions are amplified with decreasing Pt content, one would expect more significant band narrowing, stronger moment enhancement for the AF alignment, and, therefore, a higher exchange energy gain benefiting the AF ordering. On the other hand, the decreasing Fe-Pt charge transer will cause more antibonding Fe states to be occupied (see Fig. 7) attenuating, therefore, the energy benefit of covalency in the AF state. All of these changes are expected to be minute, and their net effect is difficult to predict. Since we did not carry out AF calculations for any other phase except Pt_3Fe, we are not able to explain definitely a microsopic origin of the FM-AF transition in the Pt-Fe system.

IV. COHESIVE PROPERTIES

In order to gain insight into the cohesive properties of the alloy and to find the equilibrium lattice constants, we have calculated the electronic pressure as a function of atomic volume. The partial pressures have been calculated according to the well-known formulas of Nieminen and Hodges[51(a)] and Pettifor.[51(b)] The equation of state has been calculated from the sum of partial pressures calculated for all atoms in the unit cell t, angular momenta l, and spins σ:

$$p(v)=\frac{1}{3V}\left[\sum_t\sum_l\sum_\sigma\int^{E_F} g^t_{l\sigma}(E)S_t\Phi^{t^2}_{l\sigma}(E,S_t)[D^t_{l\sigma}(E)+l+1][D^t_{l\sigma}(E)-l]dE \right.$$
$$\left.+\sum_t\sum_l\sum_\sigma\int^{E_f} g^t_{l\sigma}(E)S_t\Phi^{t^2}_{l\sigma}(E,S_t)[E-v(S_t)-\varepsilon^{xc}_{t\sigma}+v^{xc}_{t\sigma}]S_t^2dE\right], \quad (16)$$

where $g(E)$ is the density of states, S is atomic sphere radius, V is unit cell volume of the compound, $\Phi(E,S)$ is the radial wave function, D is the log derivative of Φ, $v(S)$ is the Coulomb potential at S, and v^{xc},ε^{xc} are LDA exchange-correlation potential and energy, respectively. The bulk moduli and the equilibrium lattice constants have been obtained by fitting the equation of state $p(V)$ by the Murnaghan[52] expression:

$$p(V)=\frac{B}{b}\left[\left(\frac{V_0}{V}\right)^b-1\right]. \quad (17)$$

As a result, one obtains the atomic volume V_0, the bulk modulus B, and the b parameter, which describes the linear dependence of the bulk modulus on pressure: $B(p)=B(p=0)+bp(V)$. In this approximation, b is, therefore, equivalent to the pressure derivative of the bulk modulus dB/dp.

The numerical results are listed in Table VI and the calculated and experimental lattice constants are shown in Fig. 12. The data in Table VI differ slightly from those reported earlier in Ref. 30 because of a different interpolation procedure used. The calculated lattice constants follow quite accurately the Vegard's law. For $PtFe_3$, the usual LDA overbinding effect is observed, i.e., the calculated lattice constant is some 1.5% too small. Incidentally, inclusion of the zero-point motion pressure[53] would bring the theoretical and experimental values into very close agreement. For higher Pt concentrations and for elemental Pt, we observe the opposite effect—the calculated lattice constants are larger than the experimental ones and, for fcc Pt, the error grows to +2.7% $\{S^{calc}_{WS}=2.978$ a.u., $S^{expt}_{WS}=2.90$ a.u. [Ref. 54(a)]$\}$. Andersen *et al.*[55] have calculated the equilibrium lattice constants for fcc Rh, Pd, Ir, and Pt. Their calculated S^{eq}_{WS} for Pt is even larger than ours, and for all four elements, the calculated S_{WS} exceeds the experimental values, the error growing with the atomic number. It immediately suggests that the neglect of the spin-orbit coupling is responsible. This is supported by the recent calculations of Cade and Lee[56] for HgTe. They show that for compounds containing such heavy elements ($Z=80$ for Pt), the inclusion of the spin-orbit couplings considerably

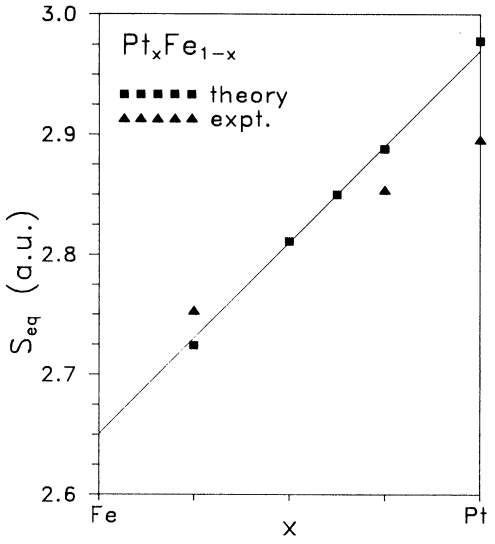

FIG. 12. Calculated and experimental equilibrium Wigner-Seitz radii for the Pt-Fe system. Experimental points refer to Refs. 62, 19(b), and 54(a).

reduces the calculated lattice constant. The calculated bulk modulus and its pressure derivative for fcc Pt ($B=2.55$ Mbar, $b=5.68$) compare fairly well with the experimental values {$B=2.78$ Mbar,[57(a)] $b=5.2$ [Ref. 57(b)]}.

Although the partial pressures depend somewhat on the S_{Pt}/S_{Fe} ratio, its constancy warrants that the observed trends are physically meaningful. We will show

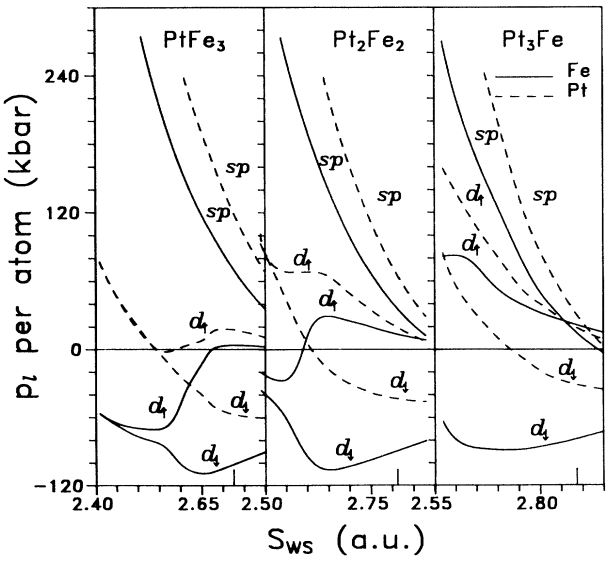

FIG. 13. Partial pressures as functions of lattice spacing for the ordered ferromagnetic phases of the Pt-Fe alloy. The *sp* components comprise *s* and *p* partial pressures for both spin directions. The vertical bars mark the calculated equilibrium Wigner-Seitz radii.

that the partial pressure analysis provide a sound and consistent picture of cohesion in the Pt-Fe system. Figure 13 displays the volume dependence of the partial pressures for all FM phases. The *sp* contributions for both spin directions have been summed up, but the *d* contributions are shown separately for both spin directions. This picture contains the most essential information on the chemical bonding in the Pt-Fe system. Before we start to analyze it, it is prudent to understand a difference in chemical bonding of Pt and Fe. The basic trends in cohesion of the 3*d*, 4*d*, and 5*d* series are well known and have been the subject of many studies.[58] It is commonly acknowledged that the gradual filling of the *d* bands is responsible for the observed parabolic behavior of the equilibrium lattice constants as a function of the atomic number, with a minimum at the middle of the series and with the corresponding maximum of the bulk modulus.[58(c)] These analyses have recently been extended in the paper by Christensen and Heine,[59] who used the decomposition of the partial pressures according to the so-called[60] "first-order pressure relations" (FOPR) in order to analyze the electronic pressure for noble metals. The FOPR were discussed in detail in Ref. 59, so we will not repeat these rather lengthy formulas here. For our purpose, it is enough to remember that two different sets of equations are used, one for the narrow (i.e., $l=2$) and the other for the free-electron-like bands (i.e., $l=0,1$), the first named "central" and the second "tail" pressures. In both sets, there are two kinds of terms: $p_{c(t)1}$, proportional to $n_l[C_l-V(S)-\varepsilon_{xc}(S)]/\mu_l$ and $P_{c(t)2}+p_{c(t)3}$, proportional to $n_l(E_l-C_l)(2l+1+2/\mu_l)$, where C_l is the canonical band center, E_l is center of the occupied part of the band, n_l is occupation number, and $V(S)$ and $\varepsilon_{xc}(S)$ are atomic sphere approximation (ASA) potential and exchange-correlation energy, respectively. For tail pressures, the band center C_l is replaced by the square-well pseudopotential V_l and μ_l by τ_l (band-bottom mass parameter). It is clear that the first term depends on the band position as a whole {with respect to $[V(S)+\varepsilon_{xc}(S)]$} for both central and tail pressures. The second term of the central pressures depends primarily on the band filling, attaining its maximum for a half-filled band. For the tail pressures, the second term can be identified as the kinetic Fermi pressure for the free-electron gas and, to a good approximation, can be treated as such for real solids.

In Table VII, the decomposed partial pressures together with relevant parameters are listed for NM fcc Fe and fcc Pt at equilibrium. We realize that the mechanisms of the chemical bonding are different in Fe and Pt. For Fe, the main attractive force comes from the $p_{c2}+p_{c3}$ term of the *d* partial pressure, since with 6.52 *d* electrons mostly the bonding states of the *d* band are occupied. The p_{c1} term is strongly repulsive, because the canonical band center C_2 is much higher than $\varepsilon_{xc}(S)$, but the net *d* partial pressure is very large and negative. For the *sp* pressures, the p_{t1} terms are negative and relatively small, since the $V_{1,2}$ pseudopotentials lay slightly lower than $\varepsilon_{xc}(S)$. The $p_{t2}+p_{t3}$ terms corresponding to the Fermi kinetic pressure are positive and large, which is not surprising, since the lattice constant of NM fcc Fe is small, and

TABLE VII. Partial pressures and their decomposition according to the first-order pressure relations for NM fcc Fe and fcc Pt. The tail pressures and the central pressures are reported for the *sp* and *d* states, respectively. The parameters listed include ε_{xc} (the exchange-correlation energy at S_{WS}), E_l [the mass center of the occupied part of the l band (Ry)], τ or μ [the effective mass parameters (m_0)], V_l or C_l [the square-well pseudopotential or canonical band center (Ry)], n_l (the band occupation), and p [the partial pressures (kbar)].

	s	*p*	*d*
NM fcc Fe, $S_{WS}=2.55$ a.u., $\varepsilon_{xc}=-0.6187$ Ry, $p_{tot}=64$ kbar			
E_l	−0.365	−0.190	−0.122
$\tau_l(\mu_l)$	0.817	0.981	8.864
$V_l(C_l)$	−0.648	−0.705	−0.039
n_l	0.645	0.832	6.52
p_1	−48	−258	603
p_2+p_3	351	683	−1426
p_{tot}	302	425	−823
p_{exact}	323	464	−781
fcc Pt, $S_{WS}=2.975$ a.u., $\varepsilon_{xc}=-0.5840$ Ry, $p_{tot}=0.4$ kbar			
E_l	−0.571	−0.395	−0.325
$\tau_l(\mu_l)$	0.904	0.968	5.619
$V_l(C_l)$	−0.834	−0.698	−0.304
n_l	0.763	0.828	8.409
p_1	−315	−274	333
p_2+p_3	285	280	−359
p_{tot}	−30	7	−25
p_{exact}	−29	10	19

the number of electron density n is large. In the case of the free-electron gas the kinetic Fermi pressure is proportional to $n^{5/3}$, and, taking into account the effective masses of the *sp* electrons being close to unity, this functional dependence should quite adequately describe the volume dependence of the $p_{t2}+p_{t3}$ terms. In effect, the equation of state for NM fcc Fe is characterized by competition of a very large inward pressure of the *d* electrons and equally large repulsion of the *sp* electrons. For fcc Pt, the number of *d* electrons is 8.41, which implies that the antibonding states of the *d* band are also partly occupied, so that the $p_{c2}+p_{c3}$ term is much less attractive. Its inward pressure is almost canceled by the p_{c1} term and is also much smaller than in NM fcc Fe due to a higher binding energy of the Pt 5*d* states as compared with the Fe 3*d* level. The net effect is a small *positive d* pressure. A similar cancellation of terms may be observed for the *sp* partial pressures. As expected, the positive kinetic Fermi pressure $p_{t2}+p_{t3}$ is smaller than for Fe, in agreement with a much larger lattice constant of Pt. It is canceled by the negative p_{t1} terms, which, particularly for the *s* partial pressure, are numerically much larger than for Fe because of the large downward shift of the V_1 pseudopotential due to the scalar relativistic corrections. We see, therefore, that in the case of fcc Pt, the partial pressures at equilibrium are all close to zero, and the crystal is kept together by *sp* electrons rather than by the *d* ones, in sharp contrast to Fe. It is a situation typical for noble metals, as discussed by Christensen and Heine[59] for Cu, Ag, and Au. We would like to point out, however, that their discussion is somewhat misleading in one aspect. In Sec. II B of their paper, they argue that the *sp* pressure in noble metals should be negative. They use the arguments based on the orderings of the characteristic energies for the *sp* band and the observation that in the half-filled band the *sp* electrons occupy predominantly the bonding states. Now, these arguments may *all* be applied to the transition metals as well, yet a real physical situation is very different there—we observe an enormous positive *sp* partial pressure at equilibrium, as shown for Fe. In our view, to set a proper picture of cohesion in transition and noble metals one must acknowledge a decisive role of *d*-band filling. The importance of this term is simply caused by a large value of n_l for the *d* shell. A large negative pressure caused by this term squeezes the lattice in the middle of the series, and since at equilibrium the total pressure must be zero by definition, a very large positive *sp* pressure must be present in these substances. For noble metals (and as we have also shown for Pt), there is no negative *d* pressure so that the *sp* pressure must also be close to zero at the equilibrium lattice constant which, of course, must assume correspondingly large values. The arguments raised by Christensen and Heine[59] explain the nature of the competition between the different terms of FOPR but cannot be used in order to predict a value of the net *sp* pressure.

The picture set above for the nonmagnetic metals gets a little more complicated for magnetic phases.[55] The bonding properties of the Fm fcc Fe have been discussed in detail in Ref. 37. The exchange interaction splits the *d* into minority and majority states. For strong ferromagnets the majority band becomes full and loses its bonding properties, increasing considerably the total pressure, the lattice constant, and compressibility.[55,58] Hence, a magnetic solid is kept together by the minority-spin electrons, their inward pressure counterbalanced by the *sp* electrons, with majority-spin *d* electrons being either weakly bonding, antibonding, or nonbonding.[37] Figure 13 shows the evolution of the binding properties of the Pt-Fe system with composition. We recognize on the figure several of the features discussed above. The most striking one is the evolution of the *d* partial pressure with volume. Appearance of the magnetic moment on Fe is reflected in a giant positive magnetic pressure, seen for both Fe $d_\uparrow$ and Pt $d_\uparrow$ pressure components. For all alloy compositions, the bonding force comes from the minority *d* electrons, with the Fe contribution per atom roughly twice as large as the Pt contribution. All other partial pressures are positive for all alloy compositions at equilibrium. The repulsive force is dominated by the Pt *sp* partial pressure, although for Pt_3Fe the positive $d_\uparrow$ contributions for Pt and Fe are comparable with the *sp* contribution. An overall pattern is that of interpolation between the two limiting cases described earlier for Fe and Pt: for $PtFe_3$, a balance of strongly repulsive *sp* and strongly attractive $d_\downarrow$ partial pressures is observed, whereas for Pt_3Fe, all partial pressures are numerically smaller, except for the positive $d_\uparrow$ pressures, with *sp* pressures close to zero. Analyzing the FOPR for the *sp* pressures at equilibrium,

we found that a decrease in their value throughout the series is caused by a decrease of the Fermi kinetic pressure $p_{t2}+p_{t3}$, the p_{t1} term being practically constant both for Pt and Fe. Also, at a given lattice constant, the *sp* $p_{t2}+p_{t3}$ terms do not vary appreciably with alloy composition. This demonstrates a close relationship between the *sp* partial pressure, in general, and its $p_{t2}+p_{t3}$ component, in particular, and the lattice constant of the alloy. Further observations that call for a microscopic explanation are a negative bulk modulus of the Fe $d_\downarrow$ partial pressure at equilibrium and an upward shift of the *d* partial pressures with growing Pt content. The behavior of the Fe $d_\downarrow$ partial pressure at equilibrium is dominated by the p_{c2} term. Since $E_2 < C_2$, this term is negative. Under compression, the effective mass μ_2 decreases, $E_2 - C_2$ slightly decreases, and the n_2 (the number of the minority electrons) increases under compression, since the magnetic moment decreases. Hence, the p_{c2} term numerically increases, giving a negative partial bulk modulus. At higher compressions, the minority band fills up and a decreasing $E_2 - C_2$ outweighs the changes in $n_{2\downarrow}$ and μ_2, making the partial bulk modulus positive.

An upward shift of both Fe and Pt *d* partial pressures with growing Pt content is a consequence of the evolution of electronic structure of the Pt-Fe system depicted in Fig. 7 and discussed in detail in Sec. III C. A main reason for the observed changes is an increase of the intrinsic effective mass of $d_\uparrow$ and $d_\downarrow$ bands of both atoms (Table V) and lowering of the band centers (Table III). These effects influence both the repulsive p_{c1} and the attractive $p_{c2}+p_{c3}$ terms. The p_{c1} terms decrease for two reasons: first, the value of $[C - V(S) - \varepsilon_{xc}(S)]$ decreases because of the band lowering and, second, because it is inversely proportional to the growing effective mass μ. The evolution of this term is opposite to the observed net changes of the *d* partial pressure. Although the $p_{c2}+p_{c3}$ term is called a band-filling term, the changes of its value upon alloy composition change are not related to the band filling. The $p_{c2}+p_{c3}$ pressures increase (become less attractive) partly because the effective masses increase (effective mass variation also influences the p_{c1} term, which is, however, repulsive, so that these two contributions partially cancel) and partly due to the decreasing vlaue of $(E_2 - C_2)$, which, in turn, results from decreasing bandwidth. The changes in $p_{c2}=p_{c3}$ outweigh the changes in p_{c1} by a factor of 1.5–2.5 for the four different *d* bands, leading to the situation shown in Fig. 13.

The calculated bulk moduli and their pressure dependence are reprted in Table VI. One observes a softening of the alloy with decreasing Pt content. We have mentioned a quite good agreement of the calculated and experimental bulk modulus of fcc Pt. We note also an excellent agreement for $PtFe_3$. The value of *B* reported by Mori and Oomi[46] for $T=0$ equals to 1.95 ± 0.05 Mbar, as compared with the calculated 1.96 Mbar. The value calculated for the NM phase of $PtFe_3$ is larger by 1.2 Mbar. We note also that the value of dB/dp for FM $PtFe_3$ differs significantly from the *B* pressure coefficients for other phases.

In order to complete the picture of cohesion of the Pt-Fe alloy, we have examined the partial contributions to the bulk modulus. To carry out this analysis we have generalized the Murnaghan equation of state[52] to the case of partial pressures. Since a partial pressure at equilibrium p_0^i is nonzero, the generalized equation reads

$$p^i(V)=\frac{B_0^i+b^i p_0^i}{b^i}\left[\left(\frac{V_0}{V}\right)^{b^i}-1\right]+p_0^i \ , \tag{18}$$

with the partial bulk modulus at V_0

$$B^i(V_0)=B_0^i+b^i p_0^i \ . \tag{19}$$

Equation (18) can be fitted to the partial pressures in order to find B_0^i, b^i, and p_0^i; V_0 having been found earlier from the fit of the standard expression [Eq. (17)] to the total pressure. Of course, $\sum_i B^i(V_0)=B$ and $\sum_i p_0^i=0$. The results of such an analysis can be summarized as follows.

(a) The partial bulk modulus for Fe is constant throughout the series and equals 0.35 Mbar. This enables one to estimate the modulus of the HS phase of fcc Fe to be (4) $0.35=1.4$ Mbar.

(b) As expected, the *sp* bulk modulus of Fe decreases throughout the series, this decrease being compensated for by increasing the *d* bulk modulus. These trends are easily understandable on the basis of the detailed discussion of partial pressures presented above. Since the behavior of the *sp* partial pressure is dominated by Fermi kinetic pressure, its bulk modulus is expected to vary as $n^{5/3}$ and should decrease with increasing lattice constant. The *d* pressure becomes less attractive ($d_\downarrow$ electrons) or more repulsive ($d_\uparrow$ electrons) and its partial bulk modulus increases from $PtFe_3$ to Pt_3Fe.

(c) The partial bulk modulus for Pt is large and ranges from 0.87 Mbar for $PtFe_3$ to 0.7 Mbar for Pt_3Fe. The trends in the partial *sp* and *d* bulk moduli are identical as for Fe and can be explained in the same way. The partial bulk moduli for Pt are, however, larger than their Fe counterparts. This is of no surprise, since the Pt partial pressures themselves are larger than the Fe partial pressures. Accordingly, Pt *sp* partial bulk modulus is $\sim 50\%$ larger than that of Fe. Moreover, there is no negative Pt $d_\downarrow$ bulk modulus, in contrast to the Fe $d_\downarrow$ contribution. This is so because the small magnetic moment of Pt is not so sensitive to the pressure. Increased occupation of the minority band has been shown to be responsible for the negative bulk modulus of the Fe $d_\downarrow$ partial pressure. This increase is not large enough for the Pt $d_\downarrow$ band and its partial bulk modulus remains positive. All of these differences make the partial bulk modulus of Pt much larger than that of Fe. This is in agreement with the discussion of the partial pressures and chemical binding: the equilibrium lattice constant results from a competition between the Fe, $d_\downarrow$ attraction and the Pt *sp* repulsion.

(d) It is noteworthy that the bulk modulus of $PtFe_3$ is dominated by the *sp* contribution, which is responsible for $\sim 64\%$ of the total value. For Pt_3Fe, the *sp* contribution accounts for $\sim 31\%$ of the bulk modulus.

(e) Since the partial bulk moduli of Fe and Pt are very

different, and their variation with alloy composition is weak, the total bulk modulus of the $Pt_{1-x}Fe_x$ system could be *grosso modo* described by the weighted mean of the Pt and Fe values: $B_{tot}=4[xB_{Fe}+(1-x)B_{Pt}]$. This is the most important reason for alloy softening with decreasing Pt content.

The discussion in the present section gives a complete and consistent description of the basic cohesive properties of the Pt-Fe system. The total-energy calculations carried out using the FSM method is planned to be presented elsewhere.[38]

V. DISCUSSION

We wish to address a few more points on which our calculations shed a light. The first problem we wish to discuss is the magnetic homogeneity of $PtFe_3$. As pointed out by Nakamura, Sumiyama, and Shiga[5] and supported recently by measurements of the hyperfine field distribution by Abd-Elmeguid and Michlitz,[25] $PtFe_3$ is magnetically homogeneous even in the disordered phase. This can be readily understood from our calculations: the local Fe moment is largely determined by the local environment, i.e., by a number of Fe NN's. In the disordered phase of $PtFe_3$, there can be a variable number of Fe NN's, both smaller and larger than 8. As argued before, the increased Pt content (which translates in the present context into a smaller number of Fe NN's, which is 4 for Pt_2Fe_2 and 0 for Pt_3Fe) causes an increase of the Fe moment. However, the configurations with a smaller number of Fe NN's find themselves in an environment that allows for an average atomic volume smaller than their equilibrium volume. This will cancel to some extent the increase of the Fe magnetic moment caused by a lower number of the Fe NN's. A magnitude of both effects can be estimated quantitatively from Fig. 9. For a number of the Fe NN's higher than 8, a limiting case is fcc Fe which at $S_{WS}=2.725$ a.u. has a stable ferromagnetic HS phase with the moment of $2.57\mu_B$. Hence, the moment of these configurations is stabilized by a relatively large lattice constant of $PtFe_3$. This explains the magnetic homogeneity of the compound. We note that there is not such a mechanism for the Ni-Fe system[29] and suspect that the other maxima observed[61] in the hyperfine field distribution for this alloy are correlated with few configurations having number of Fe NN's larger than 8.

Nakamura *et al.*[5] have found that the average value of the hyperfine field is composition independent. Hesse, Nölle, and Körner[62] have shown in a more recent paper that the mean hyperfine field actually decreases with a growing Pt content. This is an unexpected result, since we know that local Fe magnetic moment increases. Hesse, Nölle, and Korner[62] offer an explanation based on the assumption that the change of atomic volume with composition is responsible for the observed dependence. We do not think that their conclusion is correct. In our view, the observed dependence is caused by a change of the Fe 4*s* magnetic moment with alloy composition. Using, as we do, the frozen-core approximation, we are not able to calculate the hyperfine field explicitly. Ebert *et al.*[63] calculated the composition-dependent hyperfine field on Fe and Ni for Ni-Fe alloy. They found that the Fe 4*s* moment is negative for high Fe concentrations and changes sign when Fe concentration decreases. The calculated 4*s* hyperfine fields are proportional to 4*s* moment in Ni-Fe alloy.[63] For the Pt-Fe system, the Fe 4*s* moments are -0.0083, 0.0024, and $0.0138\mu_B$ for $PtFe_3$, Pt_2Fe_2, and Pt_3Fe, respectively. Using the (positive) proportionality constant calculated by Ebert *et al.*,[63] we obtain 4*s* contributions to B_{eff} equal to -40, $+12$, and $+66$ kG for the three phases. Taking the extrapolated hyperfine field at 25% of Fe (Ref. 62) as -373 kG and subtracting the 4*s* contribution, one obtains for the core contribution a proportionality constant equal to -131 kG/μ_B, a very crude estimate indeed, but not so far away from the calculated[63] value of -98 kG/μ_B for Fe in Ni-Fe. Interpolating linearly the values for $PtFe_3$ and Pt_2Fe_2, we obtain, for the composition change between 75% and 65% of Fe, a change of $+17$ kG, as compared with the measured value[62] of $\sim+8$ kG. This would imply that the field caused by the core polarization changes by ~-9 kG in this composition range. Since for core polarization, the proportionality constant is negative, such a change is consistent with a growing Fe local moment. We conclude, therefore, that the observed composition dependence of the average hyperfine field results from a strongly composition-dependent polarization of the Fe 4*s* electrons. In competition with growing core polarization, the former effect outweighs the latter and the hyperfine field decreases.

As mentioned in the Introduction, it is widely accepted today that the basic Invar mechanism is connected with the existence of two energetically nearly degenerate but magnetically different states, commonly referred to as the high-spin and low-spin phases. Recently, attempts have been made to combine the results of the band-structure calculations and of the spin-fluctuation theory in order to describe Invar behavior.[64,65,21] Wagner[64] has shown that although for a full description of the thermodynamics a complete binding-energy surface is necessary, in the simplest approximation, the mechanism of the coupled volume and spin fluctuations is specified by the energy difference between the HS and LS phases and the difference of the respective atomic volumes. The energy difference between the HS and LS phases is the most important parameter of the binding surfaces calculated by means of the FSM method.[36] Although the theoretical values are known by now for many elemental metals[26,66] and for Fe_3Ni,[65] there is no experimental verification of them. However, the recent pressure experiment by Abd-Elmeguid and Micklitz[25] brings the crucial information that makes it possible to estimate the HS-LS energy difference for $PtFe_3$. This experiment proved unambiguously the existence of the HS and LS phases for this substance. The critical pressure of 6 GPA at which the transition from the HS to LS phase occurs has been found. We have shown in a model calculation[30] that both phases can be identified using the FSM method. The total energies calculated for the LS and NM phases are very similar so, for simplicity, we will take here the properties of the NM phase as being representative for the LS phase. Taking the pressure as an independent variable in the

Murnaghan state equation, one arrives at the following expression for the total energy as a function of pressure:

$$E(p)=\frac{V_0}{(pb/B+1)^{1/b}}\frac{p+B}{b-1}+\text{const} . \quad (20)$$

If we take the values of the bulk moduli B and the b parameters for the FM and NM phases of $PtFe_3$, calculate $E_{FM}(p)$ and $E_{NM}(p)$, and form the difference $\Delta E=E_{FM}-E_{NM}$ neglecting the unknown constant terms, we obtain the curves plotted in Fig. 14. We realize now that the value of $\Delta E(p_c)$ is equal to $E_{FM}(0)-E_{NM}(0)$, i.e., to the sought energy difference of the HS and LS phases. For critical pressure $p_c=6$ GPa, this difference is only 0.2 mRy/atom for $PtFe_3$. Quite similar results have been obtained for the Ni-Fe system.[29,38] Since the quoted estimate is based solely on the well-defined experimental value of p_c and on the calculated elastic properties that agree fairly well with experiment, we believe that the estimated value is rather accurate. It seems to be smaller than previously suspected.[65,21] We claim that, if the ΔE were larger than ~ -0.7 mRy/atom, one would not be able to detect any phase transition in pressure experiments at all, simply due to the technical limitations.

The last aspect of our results we want to discuss is yet another qualitative difference between the Pt-Fe system and other isoelectronic Invar systems Pd-Fe and Ni-Fe. It is known[9] that for the Pd_xFe_{1-x} system the γ-α transition occurs at $x\cong 30$ at. %, i.e., for lower Fe concentration than in the Pt-Fe alloy. The Invar syndromes are observed at concentrations close to the transition line but in a concentration range slightly larger than for Pt-Fe. This trend is amplified for Ni-Fe, where some Invar syndromes (e.g., specific-heat anomalies) are observed for Fe concentrations as low as 50 at. %. We believe that one can understand this trend even without carrying out any calculations for Pd-Fe and Ni-Fe systems. As discussed in Sec. III C, there are three moment-enhancing mechanisms for the Pt-Fe system: covalency effects, increased lattice constant, and scalar relativistic effects. Of these, the two latter will be attenuated for Pd-Fe and will become ineffective for Ni-Fe, while the first one will be amplified. In our view, the γ-α transition occurs for Fe intermetallic alloys always when the fcc structure is not more able to support the high-spin phase. Since the moment-enhancing mechanisms are strongest for the Pt-Fe system, the fcc phase can be sustained for the highest Fe concentrations for this alloy. The discussed connection between the Invar and the strong-to-weak magnetism transition explains why the Invar concentrations are so close to the γ-α transition line. Further, the effectiveness of the moment-enhancing mechanisms in Pt-Fe confines the Invar anomalies to a very narrow concentration range. For the Pd-Fe system, the evolution towards strong ferromagnetism will be slower and even more so for the Ni-Fe system, so that the Invar anomalies for this last alloy are present in a relatively broad concentration range.

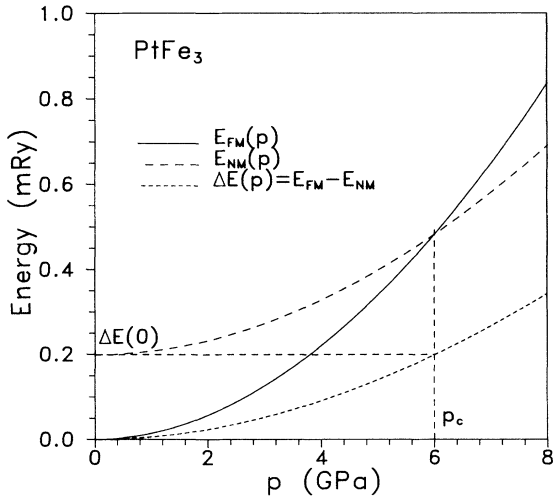

FIG. 14. Total energy calculated [Eq. (20)] as a function of pressure for nonmagnetic and ferromagnetic phases of $PtFe_3$. The two curves are shifted so that they cross at the experimental critical pressure. The difference $E_{FM}(0)-E_{NM}(0)$ is equal to the value of $\Delta E(p_c)$ calculated under the assumption that $E_{FM}(0)=E_{NM}(0)$ and gives the total energy difference between the high-spin and low-spin phase of $PtFe_3$.

VI. SUMMARY

An extensive study of the electronic structure of the Pt-Fe alloy has been carried out by means of the self-consistent LMTO method. The densities of states and the ground-state properties have been calculated for several alloy compositions and magnetic orderings. In all cases, the ordered (super)cells have been used. The volume dependence of magnetic properties, the elastic and cohesive properties, and the chemical bonding have been thoroughly discussed for several alloy compositions. In general, the calculated properties agree well with the existing experimental data. We have discussed the nature of the magnetic state of $PtFe_3$ and explained why this compound is magnetically homogeneous. The evolution of the Pt-Fe alloy from the itinerant to the local-moment system has been described from the point of view of band theory. In this contest, the issues of covalency, charge transfer, and electronegativity have been addressed. The importance of scalar relativistic effects for magnetic-moment enhancement has been pointed out. It has been shown also how one can estimate the energy difference between the HS and LS phases of $PtFe_3$ by combining the calculated equations of state and the results of Mössbauer pressure experiments. We believe that the results presented form a complete and consistent picture of the electronic structure of the Pt-Fe system, which, we hope, will be useful for forthcoming experimental and theoretical applications.

ACKNOWLEDGEMENTS

I wish to acknowledge stimulating discussions with Dr. Abd-Elmeguid, Dr. V. L. Moruzzi, Professor K. Schwarz, Professor D. Wagner, and Professor, E. F. Wassermann. This work has been supported by Deutsche Forschungsgemeinschaft under Sonderforschungsbereich 166 and by the Polish Academy of Science Grant No. CPBP 0.12.4.14.

[1]M. Hayase, M. Shiga, and Y. Nakamura, Phys. Status Solidi B **46**, K117 (1971).
[2]K. Sumiyama, M. Shiga, Y. Kobayashi, K. Nishi, and Y. Nakamura, J. Phys. F **8**, 1281 (1978).
[3]O. Caporaletti, G. M. Graham, and K. Sumiyama, J. Magn. Magn. Mater. **10**, 136 (1979).
[4]O. Caporaletti and G. M. Graham, J. Magn. Magn. Mater. **22**, 25 (1980).
[5]Y. Nakamura, K. Sumiyama, and M. Shiga, J. Magn. Magn. Mater. **12**, 127 (1979).
[6]K. Sumayama, Y. Emoto, M. Shiga, and Y. Nakamura, J. Phys. Soc. Jpn. **50**, 3296 (1981).
[7]E. F. Wassermann, Adv. Solid State Phys. **27**, 85 (1987).
[8]E. F. Wassermann, Phys. Scr. T **25**, 209 (1989).
[9]E. F. Wassermann, in *Ferromagnetic Materials,* edited by K. H. J. Buschow and E. P. Wohlfarth (North-Holland, Amsterdam, 1990), Vol. 5, p. 238.
[10]W. F. Schlosser, J. Phys. Chem. Solids **32**, 939 (1971).
[11]T. Jo, J. Phys. Soc. Jpn. **40**, 715 (1976).
[12]E. P. Wohlfarth, Phys. Lett. **28A**, 569 (1969).
[13]M. Shimizu, J. Magn. Magn. Mater. **10**, 231 (1979).
[14]S. F. Dubinin, S. K. Sidorov, and E. Z. Valiev, Phys. Status Solidi B **46**, 337 (1971).
[15]A. R. Williams, V. L. Moruzzi, C. D. Gelatt, Jr., J. Kübler, and K. Schwarz, J. Appl. Phys. **53**, 2019 (1982); A. R. Williams, V. L. Moruzzi, C. D. Gelatt, Jr., and J. Kübler, J. Magn. Magn. Mater. **31-34**, 88 (1983).
[16]T. Moriya, in *Spin Fluctuations on Itinerant Electron Magnetism,* in Vol. 56 of *Springer Series in Solid State Sciences* (Springer-Verlag, New Yori, 1985), p. 199.
[17]D. G. Pettifor and D. M. Roy, Solid State Commun. **27**, 677 (1978).
[18]J. Inoue and M. Shimzu, J. Phys. F **13**, 2677 (1983).
[19](a) A. Hasegawa, J. Phys. Soc. Jpn. **54**, 1477 (1985); (b) N. I. Kulikov, E. O. Kulatov, and S. I. Yakchimovich, J. Phys. F **15**, 1127 (1985).
[20]V. L. Moruzzi, A. R. Williams, K. Schwarz, and J. Kübler (private communication).
[21]P. Entel and M. Schröter, Physica B **161**, 160 (1989).
[22]O. K. Andersen, Phys. Rev. B **12**, 3060 (1975).
[23]H. L. Skriver, *The LMTO Method,* Vol. 41 of *Springer Series in Solid State Sciences* (Springer-Verlag, New York, 1984).
[24]S. H. Vosko, L. Wilk, and M. Nusair, Can. J. Phys. **58**, 1200 (1983).
[25]M. M. Abd-Elmeguid and H. Micklitz, Phys. Rev. B **40**, 7395 (1989).
[26]V. L. Moruzzi, P. M. Marcus, K. Schwarz, and P. Mohn, Phys. Rev. B **34**, 1784 (1986).
[27]G. L. Krasko, Phys. Rev. B **36**, 8565 (1987).
[28]M. Podgórny, Physica B **161**, 105 (1989).
[29]M. Podgórny, Acta Phys. Pol. A **78**, 941 (1990).
[30]M. Podgórny, Physica B **161**, 110 (1989).
[31]K. Schwarz, P. Mohn, P. Blaha, and J. Kübler, J. Phys. F **14**, 2569 (1984).
[32]O. K. Andersen, H. L. Skriver, H. Nohl, and B. Johansson, Pure Appl. Chem. **52**, 93 (1979).
[33]O. K. Andersen, W. Klose, and H. Nohl, Phys. Rev. B **17**, 1209 (1978).
[34]V. L. Moruzzi, P. M. Marcus, Phys. Rev. B **38**, 1613 (1988).
[35](a) E. Kisker, E. F. Wassermann, and C. Carbone, Phys. Rev. Lett. **58**, 1784 (1987); (b) C. Carbone, E. Kisker, K.-H. Walker, and E. F. Wassermann, Phys. Rev. B **35**, 7760 (1987).
[36]A. R. Williams, V. L. Moruzzi, J. Kübler, and K. Schwarz, Bull. Am. Phys. Soc. **29**, 278 (1984); K. Schwarz and P. Mohn, J. Phys. F **14**, L129 (1984).
[37]M. Podgórny, J. Magn. Magn. Mater. **78**, 352 (1989).
[38]M. Podgórny, M. Thon, D. Wagner, and J. Goniakowski (unpublished).
[39]R. Alben, J. I. Budnick, and G. S. Cargill III, *Metallic Glasses* (American Society for Metals, Metal Park, Ohio, 1978), p. 304.
[40]A. P Malozemoff, A. R. Williams, and V. L. Moruzzi, Phys. Rev. B **29**, 1620 (1984).
[41]J. Kübler, Physica B **127**, 257 (1984).
[42]K. Terakura and J. Kanomori, Prog. Theor. Phys. **46**, 1007 (1971); K. Terakura, J. Phys. F **6**, 1385 (1976); Physica B **91**, 162 (1977).
[43]R. S. Mulliken, J. Chem. Phys. **46**, 497 (1949).
[44]J. C. Slater, *Advances in Quantum Chemistry,* edited by P. O. Löwdin (Academic, New York, 1972), Vol. 6, p. 1.
[45]D. Liberman, J. T. Waber, and D. T. Cromer, Phys. Rev. **137**, A27 (1965).
[46]G. Oomi and N. Mori, J. Phys. Soc. Jpn. **50**, 2917 (1981).
[47]K. Hayashi and N. Mori, Solid State Commun. **38**, 1057 (1981).
[48]D. Bagayoko and J. Callaway, Phys. Rev. B **28**, 5419 (1983).
[49]P. Steinbach, R. A. Brand, and W. Keune, J. Magn. Magn. Mater. **70**, 102 (1987).
[50]G. E. Bacon and J. Crangle, Proc. R. Soc. London, Ser. A **272**, 387 (1963).
[51](a) R. M. Nieminen and C. H. Hodges, J. Phys. F **6**, 573 (1976); (b) D. G. Pettifor, Commun. Phys. **1**, 141 (1976).
[52]F. D. Murnaghan, Proc. Natl. Acad. Sci. U.S.A. **80**, 244 (1944).
[53]V. L. Moruzzi, J. F. Janak, and K. Schwarz, Phys. Rev. B **37**, 790 (1988).
[54]W. B. Pearson, *Handbook of Lattice Spacings and Structures of Metals and Alloys* (Pergamon, Oxford, 1964).
[55]O. K. Andersen, J. Madsen, J. K. Poulsen, O. Jepsen, and J. Kollar, Physica B **86-88**, 249 (1977).
[56]N. A. Cade and P. M. Lee, Solid State Commun. **56**, 637 (1985).
[57](a) K. A. Gschneider, Solid State Phys. **16**, 295 (1964); (b) R. Grover, I. C. Getting, and G. G. Kennedy, Phys. Rev. B **7**, 567 (1973).
[58](a) D. G. Pettifor, J. Phys. F **4**, 613 (1977); (b) V. L. Moruzzi, J. F. Janak, and A. R. Williams, *Calculated Electronic Properties of Metals* (Pergamon, New York, 1978); (c) J. F. Janak and A. R. Williams, Phys. Rev B **14**, 4199 (1976).
[59]N. E. Christensen and V. Heine, Phys. Rev. B **32**, 6145 (1985).
[60]A. R. Mackintosh and O. K. Andersen, in *Electrons at the Fermi Surface,* edited by M. Springford (Cambridge University Press, Cambridge, England, 1979).
[61]M. M. Abd-Elmeguid, B. Schleede, and H. Micklitz, J. Magn. Magn. Mater. **73**, 253 (1988).
[62]J. Hesse, G. Nölle, and H. Körner, Solid State Commun. **46**, 721 (1983).
[63]H. Ebert, H. Winter, B. L. Gyorffy, D. D. Johnson, and F. J. Pinski, J. Phys. F **18**, 719 (1988).
[64]D. Wagner, J. Phys. Cond. Matter **1**, 4635 (1989).
[65]P. Mohn, K. Schwarz, and D. Wagner, Physica B **161**, 153 (1989).
[66]V. L. Moruzzi, P. M. Marcus, and P. C. Pattnaik, Phys. Rev. B **37**, 8003 (1988); V. L. Moruzzi and P. M. Marcus, *ibid.* **38**, 1613 (1988); **39**, 471 (1989); M. Podgórny and J. Goniakowski, *ibid.* **40**, 6683 (1990).